The Astrophysical Journal, 738:187 (17pp), 2011 September 10 doi:10.1088/0004-637X/738/2/187

FORMATION AND EVOLUTION OF THE DISK SYSTEM OF THE MILKY WAY: [α/Fe] RATIOS AND KINEMATICS OF THE SEGUE G-DWARF SAMPLE

Young Sun Lee[1], Timothy C. Beers[1], Deokkeun An[2], Željko Ivezić[3], Andreas Just[4], Constance M. Rockosi[5], Heather L. Morrison[6], Jennifer A. Johnson[7], Ralph Schönrich[8], Jonathan Bird[7], Brian Yanny[9], Paul Harding[6], and Helio J. Rocha-Pinto[10,11]

[1] Department of Physics & Astronomy and JINA (Joint Institute for Nuclear Astrophysics), Michigan State University, East Lansing, MI 48824, USA; lee@pa.msu.edu, beers@pa.msu.edu
[2] Department of Science Education, Ewha Womans University, Seoul 120-750, Republic of Korea
[3] Astronomy Department, University of Washington, Box 351580, Seattle, WA 98195-1580, USA
[4] Astronomisches Rechen-Institut, Zentrum für Astronomie der Universität Heidelberg (ZAH), Mönchhofstr. 12-14, 69120 Heidelberg, Germany
[5] UCO/Lick Observatory, Department of Astronomy and Astrophysics, University of California, Santa Cruz, CA 95064, USA
[6] Department of Astronomy, Case Western Reserve University, Cleveland, OH 44106, USA
[7] Department of Astronomy, Ohio State University, Columbus, OH 43210, USA
[8] Max-Planck-Institute für Astrophysik, Karl-Schwarzschild-Str. 1, D-85741 Garching, Germany
[9] Fermi National Accelerator Laboratory, Batavia, IL 60510, USA
[10] Universidade Federal do Rio de Janeiro, Observatório do Valongo, Lad. Pedro Antônio 43, 20080-090 Rio de Janeiro, Brazil
[11] Laboratório Interinstitucional de e-Astronomia-LIneA, Rua Gal. José Cristino 77, 20921-400 Rio de Janeiro, Brazil
Received 2011 April 15; accepted 2011 June 28; published 2011 August 25

ABSTRACT

We employ measurements of the [α/Fe] ratio derived from low-resolution ($R \sim 2000$) spectra of 17,277 G-type dwarfs from the SEGUE survey to separate them into likely thin- and thick-disk subsamples. Both subsamples exhibit strong gradients of orbital rotational velocity with metallicity, of opposite signs, −20 to −30 km s^{-1} dex^{-1} for the thin-disk and +40 to +50 km s^{-1} dex^{-1} for the thick-disk population. The rotational velocity is uncorrelated with Galactocentric distance for the thin-disk subsample and exhibits a small trend for the thick-disk subsample. The rotational velocity decreases with distance from the plane for both disk components, with similar slopes (-9.0 ± 1.0 km s^{-1} kpc^{-1}). Thick-disk stars exhibit a strong trend of orbital eccentricity with metallicity (about −0.2 dex^{-1}), while the eccentricity does not change with metallicity for the thin-disk subsample. The eccentricity is almost independent of Galactocentric radius for the thin-disk population, while a marginal gradient of the eccentricity with radius exists for the thick-disk population. Both subsamples possess similar positive gradients of eccentricity with distance from the Galactic plane. The shapes of the eccentricity distributions for the thin- and thick-disk populations are independent of distance from the plane, and include no significant numbers of stars with eccentricity above 0.6. Among several contemporary models of disk evolution that we consider, radial migration appears to have played an important role in the evolution of the thin-disk population, but possibly less so for the thick disk, relative to the gas-rich merger or disk heating scenarios. We emphasize that more physically realistic models and simulations need to be constructed in order to carry out the detailed quantitative comparisons that our new data enable.

Key words: Galaxy: disk – Galaxy: formation – Galaxy: kinematics and dynamics – Galaxy: structure

1. INTRODUCTION

The Milky Way's thick disk, first identified from fits of the vertical density profile of stars with a mix of exponential functions (Yoshii 1982; Gilmore & Reid 1983), differs in many ways from the thin disk, e.g., in its kinematics and chemical abundances.

The scale height of the thick disk is about 1 kpc, while that of the thin disk is ∼0.3 kpc. Typical thick-disk stars have generally lower net orbital rotational velocities with larger velocity dispersions (Majewski 1993; Chiba & Beers 2000; Robin et al. 2003; Soubiran et al. 2003; Parker et al. 2004; Wyse et al. 2006), possess higher [α/Fe] ratios,[12] and are older and more metal-poor than typical thin-disk stars (Bensby et al. 2003, 2005; Reddy et al. 2006; Reddy 2010; Fuhrmann 2008; Haywood 2008).

Their higher [α/Fe] ratios and older ages imply that thick-disk stars were born earlier than most thin-disk stars, in an environment of rapid star formation, and that they have likely had more time to experience dynamical heating and secular processes such as scattering by perturbations in the disk. As a result of the multiple complex processes that thick-disk stars may have experienced during their lifetimes, consensus on the nature of the formation and evolution of the thick disk has yet to be reached.

The currently discussed mechanisms for thick-disk formation can be broadly divided into two groups—violent origin and secular evolution. Among the models involving violent origin, the heating scenario (e.g., Quinn et al. 1993; Kazantzidis et al. 2008) posits that the thick disk results from a pre-existing thin disk that has been dynamically heated by satellite mergers. In their simulations of this process, Villalobos & Helmi (2008) found that on the order of 10%–20% of the stars in the thickened disk component were accreted from satellites, the rest being heated thin-disk stars. The accretion origin of the thick disk (e.g., Abadi et al. 2003) invokes the hypothesis that thick-disk stars were predominantly formed in dwarf-like galaxies, which were then directly assimilated into the thick disk from orbits that reached near the Galactic disk plane. Abadi et al. (2003)

[12] The [α/Fe] ratio is often represented by an average of the [Mg/Fe], [Si/Fe], [Ca/Fe], and [Ti/Fe] ratios, which we adopt in this paper as well.

predicted that over 70% of thick-disk stars were accreted from such disrupted galaxies. The third model among the violent origin class is that thick-disk stars may have formed in situ through chaotic mergers of gas-rich systems, prompting simultaneous early star formation before and during the mergers (Brook et al. 2004, 2005, 2007), and that thin-disk stars formed after the merger events settled down.

Secular evolution by disk heating was first conceived by Spitzer & Schwarzschild (1953), who demonstrated that encounters with molecular clouds could increase the velocity dispersion of late type, old stars. Barbanis & Woltjer (1967) also showed that spiral structures might be the cause of the larger velocity dispersion of older stars in the solar neighborhood. These ideas had been further developed by several studies (e.g., Fuchs 2001, and references therein). Although challenged by Jenkins (1992), disk heating by secular processes have recently regained attention, both observationally and theoretically, as possible thick-disk formation scenarios.

Indeed, recent theoretical studies and simulations (Schönrich & Binney 2009a, 2009b; Loebman et al. 2011) suggested that the thick disk might not require a violent origin, but rather could have formed by cumulative secular processes associated with the radial migration of stars. According to the migration theories (Sellwood & Binney 2002; Roškar et al. 2008b), stars in the Galactic disk can radially move from the inner (outer) to the outer (inner) regions due to resonant scattering by transient spiral structure. Based on their simulations, Minchev & Famaey (2010) also suggested that long-lived spiral structures, interacting with a central bar, could be responsible for the radial movements of stars in a disk galaxy.

These proposed models predict various trends between the kinematic parameters and chemical abundances of disk-system stars, as well as between their kinematics and spatial distributions. For example, Schönrich & Binney (2009b) suggested that local, relatively metal-rich thin-disk stars, formed in the inner part of the disk and moved outward, while local metal-poor thin-disk stars were born in the outer disk and migrated inward to the solar radius, retaining information on the kinematic differences between the two populations. Thus, there should exist a gradient in the variation of rotational velocity with metallicity; evidence for such a behavior has been claimed observationally by Haywood (2008). Models of disk heating via satellite mergers (Villalobos et al. 2010) result in proposed relationships between rotational velocity and Galactocentric distance and distance from the Galactic plane. Gas-rich merger models (Brook et al. 2007) also predict a gradient of rotational velocity with Galactocentric radius for disk stars near the solar radius.

Sales et al. (2009) proposed that the distribution of orbital eccentricities for nearby thick-disk stars could be used to provide constraints on the various suggested formation models. A number of recent papers also have employed this framework to study possible origins of the thick disk, based on data from several large spectroscopic surveys. For example, Wilson et al. (2011) have explored data from the RAdial Velocity Experiment (RAVE; Steinmetz et al. 2006), while Dierickx et al. (2010) used data from the seventh public release of the Sloan Digital Sky Survey (SDSS DR7; York et al. 2000; Abazajian et al. 2009). The study of Casetti-Dinescu et al. (2011) combined RAVE data with newly available proper motions from the fourth release of the Southern Proper Motion Catalog (SPM4; Girard et al. 2011). We discuss their analyses and conclusions further below.

Most previous observational studies that have sought to test the various correlations predicted by the models mentioned above have used methods of assigning individual stars to membership in the thin- and thick-disk populations (based on a given star's location or kinematics) that introduce manifest biases that can confound interpretations (as previously noted by Schönrich & Binney 2009b and Loebman et al. 2011). As the chemical signatures of a star are substantially less variable properties than its spatial position or velocities over its lifetime, it is instead desirable to classify disk stars into their likely components according to their chemistry.

Among the various chemical abundance ratios that might be explored for this purpose, the [α/Fe] ratios appear particularly useful. These ratios can be relatively easily measured (as described below) and have been proven to well-separate thick-disk stars from thin-disk stars. It is known that, at least in the solar neighborhood (where essentially all previous studies have been conducted), thick-disk stars are on average enhanced in their [α/Fe] ratios by +0.2 to +0.3 dex relative to their thin-disk counterparts at a given [Fe/H]. Local kinematically selected thin- and thick-disk samples based on probabilistic membership assignments have confirmed this enhancement of [α/Fe] (e.g., Bensby et al. 2003; Reddy et al. 2006). Fuhrmann (1998, 2008) also demonstrated that dwarfs in his volume-limited sample could be clearly separated into two populations as a function of [Fe/H]—one associated with high [Mg/Fe] and the other with low [Mg/Fe]. The elemental abundance patterns of the stars with low [Mg/Fe] ratios and high [Mg/Fe] ratios are very similar to the kinematically selected thin- and thick-disk samples. The recent study by Nissen & Schuster (2010) demonstrated that nearby dwarfs with halo kinematics could be separated into two groups on [α/Fe]. They proposed that the high-α stars may have been born in the disk or bulge of the milky way and heated to halo kinematics by merging satellite galaxies or else were simply members of the early generations of halo stars born during the collapse of a proto-Galactic gas cloud, while the low-α stars may have been accreted from dwarf galaxies. Clearly, [α/Fe] ratios also provide valuable information on the timescales and intensities of star formation in the populations involved.

In this study, we make use of the first set of [α/Fe] ratios obtained for a large sample of low-resolution ($R \sim 2000$) spectra from the Sloan Extension for Galactic Understanding and Exploration (SEGUE; Yanny et al. 2009). As shown by Lee et al. (2011), for stars with SDSS/SEGUE spectra of signal-to-noise ratios (S/Ns) greater than 20 Å^{-1}, and with temperatures in the range 4500 K $\leqslant T_{\rm eff} \leqslant$ 7000 K, one can estimate [α/Fe] with an accuracy of better than 0.1 dex (as derived by comparing [α/Fe] estimates from the analysis of moderately high-resolution and medium-resolution spectra with those obtained from application of our methods to the same stars). This enables a *chemical separation* of the disk system into likely thin- and thick-disk populations. In this paper, we explore the observed correlations of rotational velocity and orbital eccentricity with metallicity, Galactocentric distance, and distance from the Galactic plane, as well as the orbital eccentricity distributions for the individual populations, and compare with the predictions of the radial migration, gas-rich merger, accretion, and dynamical heating models. Since we believe that direct quantitative comparisons with the predictions made by various models (or simulations) mentioned in this study are somewhat premature, we emphasize the more qualitative aspects of these comparisons.

This paper is outlined as follows. In Section 2, we present the G-dwarf sample from SEGUE, describe various cuts imposed on the sample to obtain a refined disk dwarf sample, and discuss

the calculations used to derive their space motions and orbital eccentricities. Section 3 describes how we assign membership of the stars into either the thin- or thick-disk populations. Results from our G-dwarf sample and discussion of comparisons of our results with the predictions of various contemporary disk formation and evolution scenarios follow in Sections 4 and 5, respectively. A summary and our conclusions follow in Section 6.

2. SELECTION OF LOCAL DWARF STARS

2.1. The SEGUE G-dwarf Sample

Our initial sample comprises low-resolution ($R \sim 2000$) spectra of ~63,000 stars from SDSS Data Release 8 (DR8; Aihara et al. 2011), obtained during the SEGUE sub-survey, which were originally targeted as G-dwarf candidates (with colors and magnitudes in the range $0.48 < (g-r)_0 < 0.55$ and $r_0 < 20.2$). As a result of the simple sampling function, this data set is expected to be relatively unbiased with respect to chemistry, and completely unbiased with respect to kinematics. In order to obtain a subsample of disk stars with the most reliably estimated physical quantities, we apply several additional cuts.

First, we exclude stars lacking information on their stellar parameters (effective temperature, $T_{\rm eff}$, surface gravity, $\log g$, and metallicity, [Fe/H]), radial velocities, or proper motions. The stellar atmospheric parameters were determined by the most recent version of the SEGUE Stellar Parameter Pipeline (SSPP; Lee et al. 2008a, 2008b; Allende Prieto et al. 2008; Smolinski et al. 2011); typical external errors in these estimates are 180 K in $T_{\rm eff}$, 0.24 dex in $\log g$, and 0.23 dex in [Fe/H] (Smolinski et al. 2011). It has been shown that shifts in the SSPP-derived estimates of [Fe/H] and [α/Fe] caused by the presence of unrecognized spectroscopic binaries are generally small (Schlesinger et al. 2010). Although the typical uncertainty of the radial velocity varies with the S/N of a spectrum, it is less than 5 km s^{-1} for the great majority of stars in our sample. Proper motion information was obtained based on the procedures described by Munn et al. (2004); the systematic error noted by Munn et al. (2008) has been corrected (final typical errors are 3–4 mas yr^{-1}), and we have adopted the Munn et al. recommendations for maximum fit residuals and minimum numbers of epochs considered in order to obtain the most reliable proper motions. In this regard, see also Bond et al. (2010), who investigated the systematic errors in Munn et al. (2008) by comparison with the expected null proper motions of SDSS quasars.

Distances to individual stars are estimated using a calibrated set of stellar isochrones (An et al. 2009b), following the prescription in An et al. (2009a). After correcting photometry for dust extinction, main-sequence fitting is performed simultaneously on three different color–magnitude diagrams (CMDs), with r as a luminosity index, and $g-r$, $g-i$, and $g-z$ as color indices, respectively. We adopt an SSPP-derived [Fe/H] in the distance estimation for each star, and fix a stellar age and [α/Fe] of the model at a given [Fe/H], assuming a linear relationship between [Fe/H] and these quantities (see An et al. 2009a). Distance estimates obtain using [α/Fe] from this assumption may not be internally consistent with analyses based on the SSPP-determined [α/Fe], but even a ~0.1 dex difference in [α/Fe] has a negligible impact on the derived distances (~0.01 mag in distance modulus). We also limit models in the fitting to $\log g \geqslant 4.2$ to minimize possible distance bias from stellar age effects near the main-sequence turnoff. An inter-comparison of results from the three CMDs suggests that the internal error in the distance modulus is ~0.1 mag; an additional ~0.1 mag error is expected from the combined errors in age, [Fe/H], [α/Fe], and $E(B-V)$. This suggests that the associated distance-modulus error is ~0.14 mag for individual stars. The effects of binarity are more difficult to quantify and are not included in this error estimate (see An et al. 2007; Sesar et al. 2008).

The [α/Fe] ratio is derived following the procedures described by Lee et al. (2011). Briefly summarizing, Lee et al. first generated a grid of synthetic spectra, covering 4000 K $\leqslant T_{\rm eff} \leqslant$ 8000 K in steps of 250 K, $0.0 \leqslant \log g \leqslant 5.0$ in steps of 0.2 dex, $-4.0 \leqslant$ [Fe/H] $\leqslant +0.4$ in steps of 0.2 dex, and $-0.1 \leqslant$ [α/Fe] $\leqslant +0.6$ in steps of 0.1 dex, then determined [α/Fe] by searching the grid for a synthetic spectrum that best matches a given SDSS/SEGUE spectrum (in regions that are most influenced by [α/Fe]). By comparing with a set of moderately high-resolution ($R = 15{,}000$) and medium-resolution ($R = 6000$) spectra of SDSS/SEGUE stars, they demonstrated the ability to measure [α/Fe] from SDSS/SEGUE spectra (with S/N > 20 Å^{-1}) with uncertainties less than 0.1 dex, for stars with atmospheric parameters in the range $T_{\rm eff} = [4500, 7000]$ K, $\log g = [1.5, 5.0]$, and [Fe/H] = [−1.4, +0.3], over the full range of [α/Fe] considered. For stars with [Fe/H] < −1.4, slightly higher S/N was required to achieve this precision (S/N > 25 Å^{-1}).

In order to assemble a local dwarf sample, we only include stars with distances, d, less than 3 kpc from the Sun and with $\log g \geqslant 4.2$. These cuts ensure that we are selecting likely dwarfs from which we can obtain accurate space motions (i.e., that do not suffer from severe degradation due to propagation of proper motion errors at larger distances). In order to perform a confident separation of the thin- and thick-disk populations on the basis of [α/Fe], we further require that the spectra of the dwarf stars included in our analysis have S/N $\geqslant$ 30 Å^{-1}. This conservative cut on S/N ensures not only high quality estimates of [Fe/H] and [α/Fe], but also that our program stars have small errors in estimated radial velocity (less than 5 km s^{-1}).

2.2. Calculations of Space Motions and Orbital Eccentricity

With information on the distances, radial velocities, and proper motions for our program stars in hand, we then derive the U, V, W space velocity components. We apply $(U, V, W)_\odot = (11.10, 12.24, 7.25)$ km s^{-1} (Schönrich et al. 2010) to adjust for the solar peculiar motions with respect to the local standard of rest (LSR). For the purpose of our analysis, we also make use of the rotational velocity around the Galactic center in a cylindrical coordinate system, V_ϕ, calculated assuming $R_\odot = 8.0$ kpc and $V_{\rm LSR} = 220$ km s^{-1}. The Galactocentric distance projected onto the Galactic plane, R, and the vertical distance from the Galactic plane, $|Z|$, are also obtained. In addition, by adoption of an analytic Stäckel-type gravitational potential (which includes a flattened, oblate disk and a spherically shaped massive dark halo; see Chiba & Beers 2000), we compute $r_{\rm apo}$ ($r_{\rm peri}$), the maximum (minimum) distance from the Galactic center that a star reaches during its orbit, as well as the orbital eccentricity, e, defined as $(r_{\rm apo} - r_{\rm peri})/(r_{\rm apo} + r_{\rm peri})$. Errors in the derived kinematics and orbital parameters for each star due to propagation of the errors in the observed quantities (mostly dominated by distance and proper motion errors) are determined by 1000 realizations of a Monte Carlo simulation.

We next remove stars from our sample with derived rotational velocities relative to the Galactic center less than

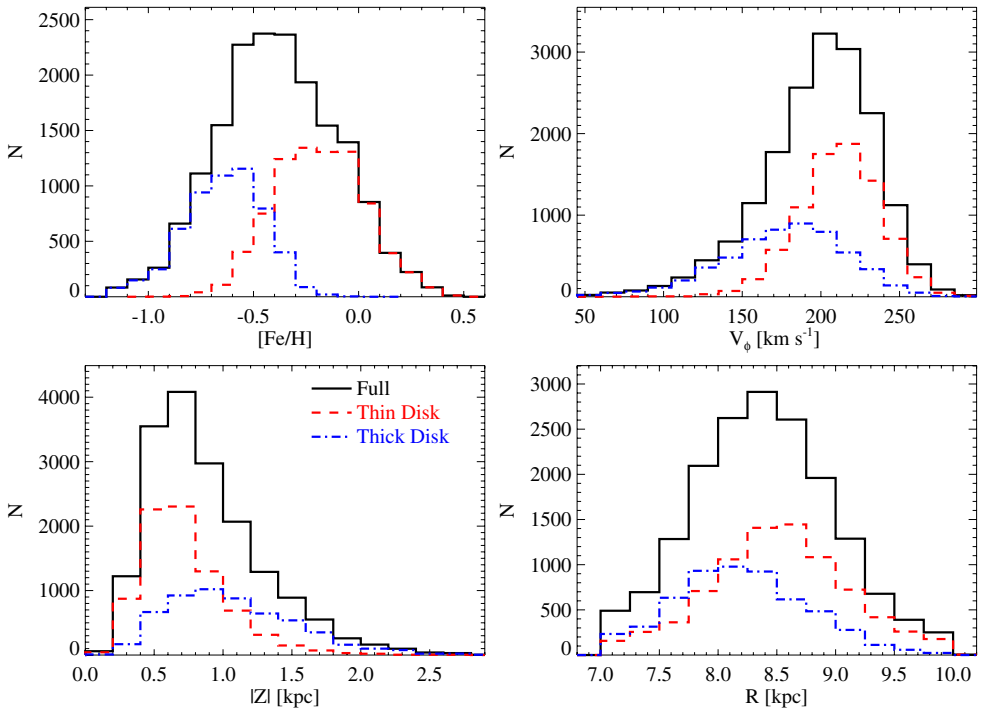

Figure 1. Distributions of metallicities, [Fe/H] (top left), rotational velocities, V_ϕ (top right), distances from the Galactic plane, $|Z|$ (bottom left), and Galactocentric distances projected onto the plane, R (bottom right) for the final selected sample. The solid line indicates our final full dwarf sample, while the dashed red and dash-dotted blue lines are the thin- and thick-disk subsamples, respectively, with stars assigned by the procedures described in Section 3.

$V_\phi = +50$ km s^{-1}, with [Fe/H] $\leqslant -1.2$, and located outside the range 7 kpc $< R <$ 10 kpc, in order to minimize contamination from the halo and outer-disk components.

Finally, we perform a simple check on the likely remaining halo contamination in our sample following the prescription of Bensby et al. (2003). For calculation of the approximate disk and halo star fractions (assuming our data are representative of the local solar neighborhood densities), we adopt the local stellar densities, velocity dispersions in U, V, and W, and the asymmetric drifts listed in their Table 1, assuming the space velocities of the thin-disk, thick-disk, and halo stars are distributed as Gaussians. Based on these probability distributions, we reject stars that have greater likelihood of belonging to the halo than to the disk system. This check removes only about 59 additional stars from the sample, showing that the above selection criteria for thin- and thick-disk stars are quite reasonable. We also experimented with the application of slightly different scale heights for describing the variation of halo stellar densities with $|Z|$, but the above result appears quite robust. Note, however, that these various cuts do not necessarily eliminate contamination by members of the so-called metal-weak thick-disk (MWTD) population, which Carollo et al. (2010) have shown exhibits metallicities in the range $-1.7 <$ [Fe/H] < -0.7, and a prograde rotation of $V_\phi \sim +100$ to +150 km s^{-1}. We comment on any evidence for MWTD contamination below.

Summarizing the criteria used for our sample selection, surviving program stars satisfy $d < 3$ kpc, $\log g \geqslant 4.2$, S/N $\geqslant 30$ Å^{-1}, $V_\phi > +50$ km s^{-1}, [Fe/H] > -1.2, 7 kpc $< R <$ 10 kpc, and possess greater probability of belonging to the disk system than to the halo. The surviving sample from the above cuts contains ~17,300 stars. Figure 1 shows the distributions of [Fe/H], V_ϕ, $|Z|$, and R for the final dwarf sample (solid lines), before and after further division based on the derived [α/Fe] ratios into the thin- and thick-disk populations, as described below. Note that the bottom left panel of Figure 1 has only a small number of stars with $|Z| < 0.2$ kpc, owing to the bright limit of SDSS imaging ($g > 14.0$). Thus, our analysis in the following sections may be only valid for the thin-disk population with $|Z| > 0.2$ kpc, rather than the young(er) thin disk closer to the plane.

3. DIVISION OF THE SAMPLE ON [α/Fe] INTO THIN- AND THICK-DISK POPULATIONS

3.1. Dividing Scheme and its Efficiency

As mentioned previously, since a stellar population's kinematics and spatial distributions can be modified over time (especially in the disk system), while a (dwarf) star's atmospheric chemical abundance is essentially invariant (except in unusual circumstances, such as binary mass transfer from an evolved companion), we make use of the estimated [α/Fe] ratio as a reference to separate the thin- and thick-disk populations. This choice is also strongly motivated by the apparent bi-modal distribution of stars in the [α/Fe] and [Fe/H] plane seen in Figure 2.

For the purpose of the present analysis, our dwarf sample is split into likely thin-disk (with low [α/Fe]) and thick-disk (with high [α/Fe]) populations, based on the following scheme.

1. For stars with [Fe/H] $\geqslant -0.8$
   (a) thin disk, if [α/Fe] $< -0.08\cdot$[Fe/H] $+ 0.15$
   (b) thick disk, if [α/Fe] $> -0.08\cdot$[Fe/H] $+ 0.25$.
2. For stars with [Fe/H] < -0.8
   (a) thin disk, if [α/Fe] $< +0.214$
   (b) thick disk, if [α/Fe] $> +0.314$.

This division into the thin- and thick-disk populations is devised based on examination of the distribution of number densities in the [α/Fe] versus [Fe/H] plane, shown in Figure 2. Note how well the populations appear to separate above and below the solid line in this figure, which is our adopted fiducial.

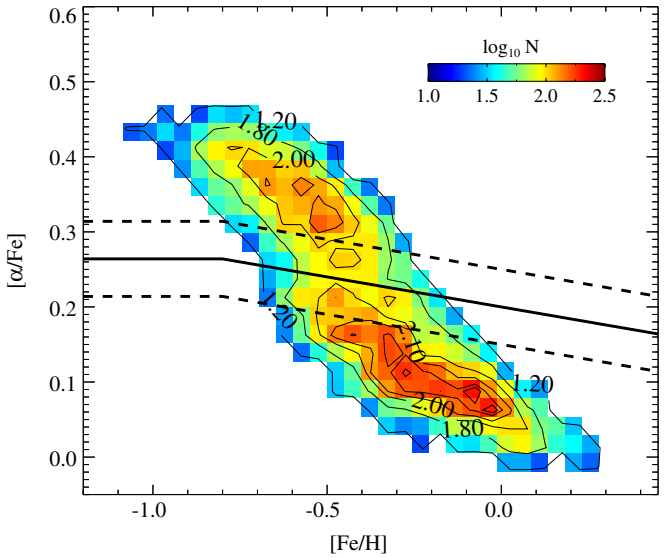

Figure 2. Distribution of logarithmic number densities, in the [α/Fe] vs. [Fe/H] plane, overplotted with equidensity contours. Each bin is 0.025 dex in [α/Fe] by 0.05 dex in [Fe/H] and is occupied by a minimum of 20 stars. The median occupancy is 70 stars. The solid line is the fiducial for division into likely thin- and thick-disk populations; the dashed lines located $\pm$0.05 dex in [α/Fe] on either side of the solid line indicate the adopted dividing points for the high-[α/Fe] (upper-dashed) and low-[α/Fe] (lower-dashed) stars in our sample.

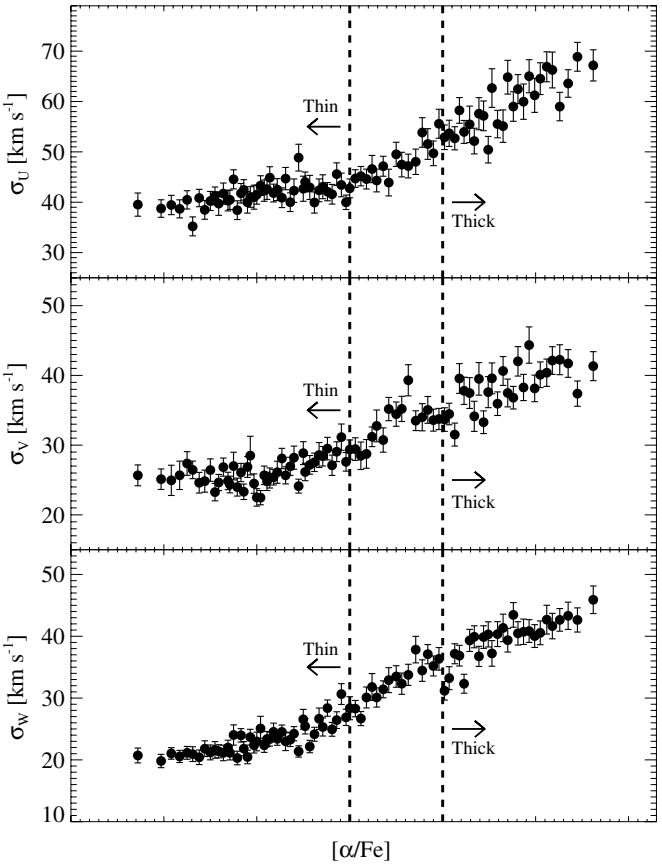

Figure 3. U, V, W velocity dispersions, as a function of [α/Fe], are shown from top to bottom, respectively. Well-defined trends of the velocity dispersions can be seen, providing kinematic confirmation that the proposed separation of the thin-disk and thick-disk populations on the basis of [α/Fe] works very well. Each dot contains 200 stars, and the error bar on each point is calculated by resampling these 200 stars with replacement 1000 times. The vertical dashed lines provide references at [α/Fe] = +0.2 and +0.3, which roughly correspond to the divisions shown in Figure 2.

The dashed lines located $\pm$0.05 dex in [α/Fe] above and below the fiducial solid line in Figure 2 indicate the dividing points for the high-[α/Fe] (thick-disk) and low-[α/Fe] (thin-disk) stars. Note that this leaves a gap of 0.1 dex in [α/Fe] between the thin- and thick-disk dividing lines. This choice serves to reduce the number of misclassified stars that may arise from observational errors in their measured [α/Fe] values. The dashed red line in Figure 1 shows the thin-disk subsample, whereas the dash-dotted blue line is for the thick-disk subsample, classified by the dividing schemes described above. From this figure, one can roughly read off the ranges and peak values of the estimated and derived parameters for each subsample.

To check on the efficacy of the chemical separation of the disk populations through use of the [α/Fe] ratio, we have investigated the variation of the U, V, W velocity dispersions of our sample with [α/Fe]. It is well known that the dispersion of each velocity component increases with distance from the Galactic plane (as well as on age, on average). In any event, the thick-disk population exhibits substantially higher dispersions than the thin-disk counterpart. Figure 3 shows the derived velocity dispersions of our sample as a function of [α/Fe]. It is readily apparent that, up to around [α/Fe] = +0.2, the dispersion of each velocity component increases moderately. Above [α/Fe] = +0.2 the gradients of the velocity dispersions with [α/Fe] become somewhat steeper. Above [α/Fe] = +0.3, the magnitude of each velocity dispersion is larger by about 10 km s^{-1} than for [α/Fe] $<$ +0.2. As our thin-disk stars mostly have [α/Fe] $<$ +0.2 and thick-disk stars possess [α/Fe] $>$ +0.3, Figure 3 kinematically confirms that the division by [α/Fe] into the thin- and thick-disk populations is quite robust.

3.2. Impact of Potential Metallicity Bias

One may be concerned about biases in our initial sample that might arise from our $(g - r)_0$ target selection due to small, but non-zero, metallicity sensitivity of the stellar colors. Haywood (2001), for example, has previously suggested that targeting stars on the basis of their spectral types (e.g., G-dwarfs) preferentially selected more metal-poor than metal-rich stars, resulting in a metallicity distribution shifted lower by about 0.1–0.3 dex.

If our selected sample strongly favors metal-poor over metal-rich stars, this bias might produce misleading correlations between the parameters we are seeking to understand. For example, at least for the thick-disk population, previous studies have indicated that the observed stellar orbital rotational velocity decreases with declining metallicity. Thus, if biases have increased the relative numbers of metal-poor stars in the thick-disk subsample, the overall distribution of V_ϕ will be shifted to lower rotational velocity. However, it should be kept in mind that, because our sample does not suffer from kinematic bias, any correlations that we are seeking between kinematics and chemical abundances will not be affected by any potential metallicity bias, as long as the correlations are derived from ranges of R and $|Z|$ that are sufficiently small such that the correlations remain roughly constant over the regions considered. Furthermore, any kinematic trends with R and $|Z|$ will not be affected by metallicity bias, as long as the metallicity distributions of stars in different ranges of the spatial cuts do not vary significantly.

Hence, instead of correcting for possible selection bias in our sample (which itself is a complex and tricky business), we instead seek to demonstrate that any presumed metallicity bias

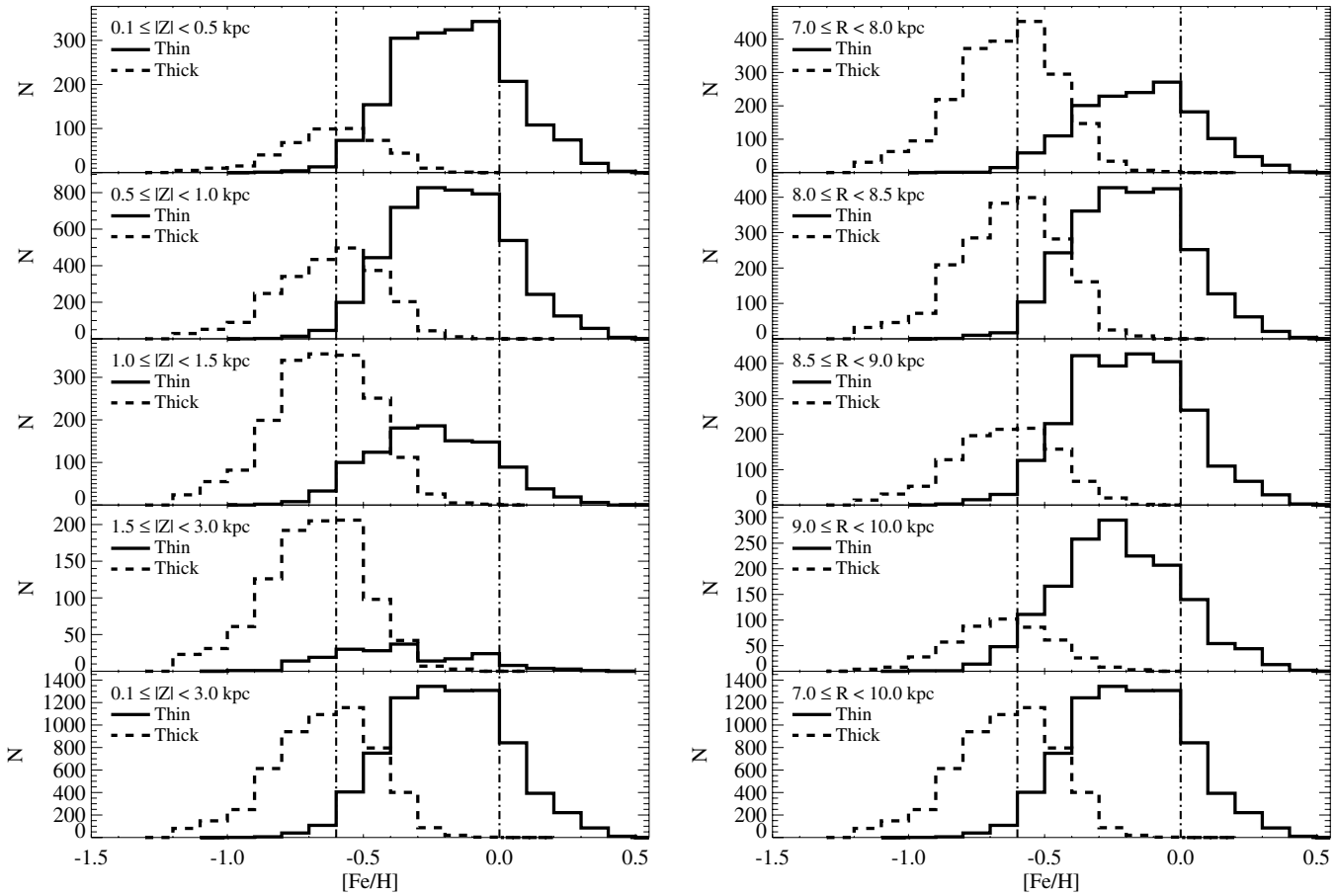

Figure 4. Distributions of metallicities in different regions of distance from the Galactic plane (left panel) and the Galactic center (right panel) for the thin-disk (solid line) and thick-disk (dashed line) subsamples. For the thin-disk subsample, as the $|Z|$ distance increases, the relative numbers of metal-poor stars slightly increases (in particular for the region $|Z| > 1.5$ kpc). For the thick-disk subsample, the metallicity distribution does not change with height above or below the Galactic midplane. The metallicity distribution mostly stays the same throughout the different cuts of Galactocentric distance for both the thin- and thick-disk subsamples. The bottom panels show the full samples of thin- and thick-disk stars, over the range 0.1 kpc $\leqslant |Z| <$ 3.0 kpc. Note that the y-axis scale is very different for each panel. The vertical dash-dotted lines are reference lines at [Fe/H] = 0.0 and [Fe/H] = −0.6.

does not greatly impact the kinematic correlations with spatial parameters that we derive by examination of the metallicity distribution functions (MDFs) for both the thin- and thick-disk subsamples in various regions of R and $|Z|$. If there is any sudden change in the MDFs of each subsample between neighboring regions, then it will be a sign that the subsample may not be suitable for deriving meaningful correlations between kinematics and distance.

For the thick disk, there is some existing evidence for the lack of a metallicity gradient with distance above the Galactic plane (e.g., Gilmore et al. 1995), or at most for only a small one, on the order of 0.1–0.2 dex kpc^{-1} (Ivezić et al. 2008). So, the shape of the observed MDFs at different heights should remain roughly constant. The left panel of Figure 4 displays the observed MDFs for both the thin- and thick-disk subsamples in different bins of $|Z|$ distance. From inspection, the relative numbers of metal-rich stars in the thick-disk subsample do not grossly change with different cuts on height above the plane, so false kinematic trends with $|Z|$ are not expected to arise. Quantitatively, the fraction of the stars with [Fe/H] < -0.6 for the thick-disk subsample is 0.51, 0.51, 0.58, and 0.64 from the first to the fourth panel, respectively (a resulting metallicity gradient with $|Z|$ of -0.029 ± 0.019 dex kpc^{-1}), consistent with the expectation from previous work. These results are also in line with the findings of Haywood (2001), who noted that the metallicity bias arising from the color selection was significant for stars with [Fe/H] > -0.2, but not for relatively metal-poor thick-disk stars.

However, this seems not to be the case for the thin-disk subsample shown in the left panel of Figure 4. At heights above $|Z| = 1.5$ kpc (already many thin-disk scale heights above the plane), we note that more metal-rich stars have dropped out of the distribution, compared with the upper three panels. This is quantitatively confirmed by examination of the fraction of stars with [Fe/H] < -0.2 (0.45, 0.46, 0.58, and 0.71 from the first to the fourth panel). This may be a natural consequence of selecting the sample without consideration of the $|Z|$ distance, since at greater heights thick-disk stars are expected to dominate. In other words, some of the stars in the metal-poor tail of the thin-disk subsample may in reality belong to the thick disk, but they have been misclassified as thin-disk stars due to errors in the estimated [α/Fe]. Indeed, considering the distribution of [α/Fe] for the stars with [Fe/H] < -0.3 and $|Z| > 1.5$ in the thin-disk subsample, many of the stars have [α/Fe] $> +0.15$. Thus, moderately α-enhanced stars at this height may mostly belong to the thick disk rather than to the thin disk, with a much lower probability of old thin-disk membership.

Simple experiments support the above argument. According to Lee et al. (2011), the error in [α/Fe] at S/N = 30 Å^{-1} is about 0.08 dex. If we assume this is a reasonable estimate of

a 1σ random error in [α/Fe] for all stars with $|Z| > 1.5$ kpc, and simultaneously perturb the measured [α/Fe] and [Fe/H] values according to a normal distribution with $\sigma = 0.08$ dex and the measured uncertainty in [Fe/H], the total number of stars classified as members of the thin-disk component falls to about 85, after averaging the results of 1000 different realizations. This is substantially smaller than the 201 stars that are claimed to be present. Thus, it is valid (within statistical fluctuations) to say that the low-[α/Fe] metal-poor thin-disk stars in this $|Z|$ distance region are likely spurious and are found at roughly the expected level of contamination. Moreover, as the total number of thin-disk stars in this most distant region is rather small, we expect the impact of such stars on our analysis to be minimal.

Concerning the variation of the MDFs for cuts in the R distance, many previous studies (e.g., Nordström et al. 2004; Holmberg et al. 2007; Andrievsky et al. 2004; Lemasle et al. 2007; Sestito et al. 2008; Magrini et al. 2009) that used open clusters and/or field stars to derive radial metallicity gradients report rather small gradients, on the order of -0.05 to -0.1 dex kpc^{-1}. Thus, we expect the MDFs in our sample to appear similar in different bins of radial distance from the Galactic center. The right panel of Figure 4 shows the MDFs of the thin- and thick-disk subsamples for several slices in R. From inspection, the overall shapes of the MDFs remain the same through the fourth panel, although there is a small drop in the numbers of thin-disk stars around [Fe/H] ~ -0.1 in the distance range 9.0 kpc $< R <$ 10.0 kpc. Calculating the fraction of the stars with [Fe/H] < -0.6 for the thick-disk subsample, we obtain 0.56, 0.54, 0.58, and 0.61 from the first to the fourth panel, a resulting radial metallicity gradient of -0.008 ± 0.004 dex kpc^{-1}. For the thin-disk subsample, the fraction of the stars with [Fe/H] < -0.2 is 0.42, 0.47, 0.48, and 0.57 from the first to the fourth panel. The derived radial metallicity gradient is -0.043 ± 0.004 dex kpc^{-1}; these slopes do not differ significantly from the previous studies. Thus, the results of these two exercises suggest that it is highly unlikely that any potential metallicity bias in our sample can greatly affect our derived kinematic correlations with R and $|Z|$.

Potential biases also might depend on the age distribution of our sample, which is not known at present, and in any case is difficult to quantify. As the narrow color range applied to originally select the G-dwarfs for spectroscopic follow-up in SEGUE also preferentially selects certain age ranges on the main sequence, we might expect that this bias might contribute at some level to the observed trends (e.g., rotational velocity versus metallicity) that we are seeking to understand. However, as noted by Haywood (2001), age bias is expected to be even less important than the metallicity bias that we have already shown to have minimal effect.

4. RESULTS OF THE OBSERVATIONS

In this section, we use our local G-dwarf sample to examine the observed gradients of V_ϕ with [Fe/H], R, and $|Z|$, as well as trends of e with [Fe/H], R, and $|Z|$ for the thin-disk and thick-disk populations as identified above.

4.1. Correlations between Rotational Velocity and Metallicity

The top panel of Figure 5 shows a color-coded distribution of V_ϕ in the [α/Fe] versus [Fe/H] plane for our G-dwarf sample. Detailed examination of this panel (as well as Figure 2) reveals a metal-poor tail for the low-[α/Fe] stars ($< +0.2$), which we associate with the thin disk, extending down to [Fe/H] $= -0.7$.

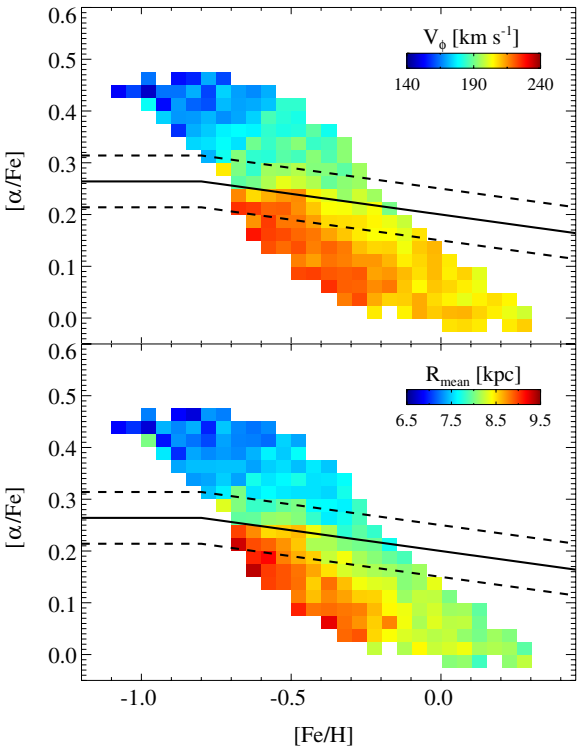

Figure 5. Distribution of rotational velocities (V_ϕ, top panel) and the average orbital radii (R_{mean}, bottom panel) for our G-dwarf sample in the [α/Fe] vs. [Fe/H] plane. As in Figure 2, the dividing lines for the thin- and thick-disk subsamples are shown. Each bin has a size of 0.025 dex in [α/Fe] by 0.05 dex in [Fe/H] and is occupied by a minimum of 20 stars. The median occupancy is 70 stars. Each bin represents a 3σ clipped mean of V_ϕ so that outliers in each bin do not significantly affect the average behavior.

This already implies that the thin disk may not be well described by a single metal-rich population with a peak around [Fe/H] $= -0.2$. We also notice from this panel that a higher rotational velocity is observed in the region of the metal-poor thin disk ([α/Fe] $< +0.2$ and [Fe/H] < -0.3), suggesting a negative trend of V_ϕ with [Fe/H]. In contrast, the high-[α/Fe] stars ($> +0.3$, which we associate with the thick disk) apparently exhibit a strong positive trend of V_ϕ with [Fe/H]. We investigate these trends quantitatively below.

The bottom panel of Figure 5 displays the distribution of mean orbital radii (R_{mean}) in the [α/Fe] versus [Fe/H] plane. It is clear that the stars we associate with the thick-disk population exhibit smaller mean orbital radii than those associated with the thin disk. In addition, the metal-poor thin-disk stars possess larger mean orbital radii than the dominant metal-rich thin-disk stars.

A recent observational study by Navarro et al. (2011) obtained a slightly different result for their thin-disk subsample. These authors found little or no correlation between V_ϕ and [Fe/H] for their thin-disk stars (defined by [Fe/H] > -0.7 and [α/Fe] $< +0.2$), although the subset of their thin-disk subsample with available Eu abundances (so that potential thick-disk or halo stars could be rejected) exhibits a very similar pattern to that which we identify here. One should also keep in mind the possibility of effects from selection biases in their sample, as it was based on an assembly of stars that included kinematically selected targets.

Haywood (2008) separated thin-disk stars with [Mg/Fe] $< +0.2$ from thick-disk stars with [Mg/Fe] $> +0.2$ in the spectroscopic sample of Soubiran & Girard (2005) and found an

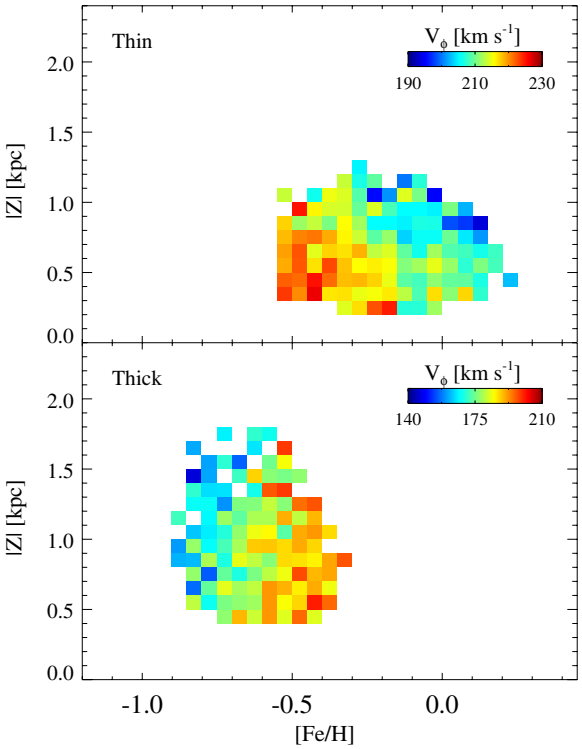

Figure 6. Distribution of rotational velocities for the low-α, thin-disk subsample (top panel) and the high-α, thick-disk subsample (bottom panel) in the $|Z|$ vs. [Fe/H] plane. As in Figure 5, each bin has a size of 0.025 dex in [α/Fe] by 0.05 dex in [Fe/H] and is occupied by a minimum of 20 stars. The median occupancy is 47 stars. Each bin represents a 3σ clipped mean of V_ϕ so that outliers in each bin do not significantly affect the average behavior.

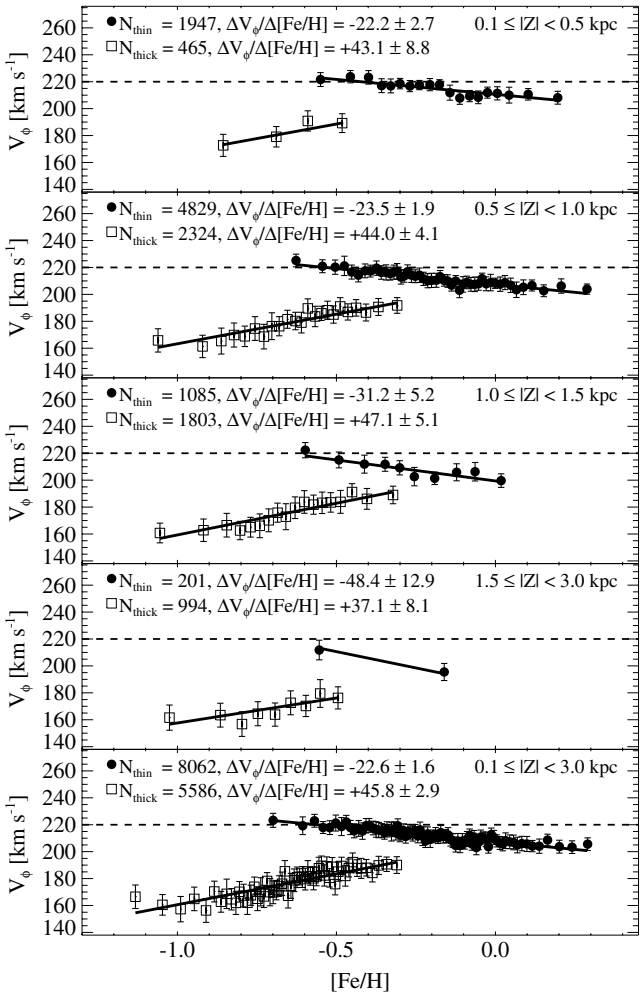

Figure 7. Rotational velocity gradients with metallicity for different slices in distance from the Galactic plane, for stars assigned to the thin-disk (black dots) and thick-disk (open squares) populations. Each dot represents a 3σ clipped average of 100 stars. Note that the 1σ error bars associated with each point are very small (on the order of 3–5 km s^{-1}), so for visualization purposes 2σ error bars are plotted instead. The error bars are calculated by resampling the 100 stars in each population (with replacement) 1000 times. The bottom panel shows the results for the full samples of stars considered. Note that although binned data are shown for clarity, estimates of the slopes and their errors are obtained for the full unbinned data (see the text).

increasing trend of the mean orbital radii with decreasing metallicity for the thin-disk population, along with a decreasing trend of mean radii with decreasing metallicity for the thick-disk population (see his Figure 3). He claimed that this tendency resulted from stars that migrated from the inner and outer disks. These behaviors are qualitatively in very good agreement with our findings in the bottom panel of Figure 5.

Rocha-Pinto et al. (2006) also reported a similar behavior between the mean orbital radii and the chemical abundances in their volume-complete sample of 325 late-type dwarfs. Their primary results were that as the difference in the distance between the mean orbital radius and the solar radius increases, the abundances of Fe, Na, Si, Ca, Ni, and Ba all decrease. This relationship between the chemical abundances and the mean orbital radii could be accounted for by radial displacements of the stars involved.

It is quite remarkable that all of the observed behaviors of the mean orbital radii from our G-dwarf sample agree so well with several previous observational studies (based on much smaller samples).

Figure 6 indicates that there exists a clear gradient of V_ϕ with [Fe/H] at any given $|Z|$ distance, for both the thin-disk subsample (top panel) and the thick-disk subsample (bottom panel). Figure 7 displays the observed gradients at different heights above the plane for both subsamples. Similar slopes of V_ϕ for both the low- and high-[α/Fe] stars are obtained for the various slices in $|Z|$ distance, although the slope of the thick-disk subsample becomes shallower at larger distance (fourth panel), and slightly steeper for the thin-disk subsample (which only includes 201 stars). The slopes are obtained by performing least-square fits to the *unbinned* samples of each population; the uncertainties in the slopes are calculated by resampling each population with replacement 1000 times. In that process, the [Fe/H] and V_ϕ values are perturbed simultaneously by draws from a normal distribution using the 1σ errors in each quantity. The data shown in the kinematic correlation plots are binned only for clarity.

If significant contamination of our thick-disk subsample by unrecognized MWTD stars were present, we might expect the slope of the correlation of V_ϕ with [Fe/H] to *increase* with distance above the plane, due to the greater velocity lag, larger scale height, and lower metallicities of the MWTD component compared with that of the canonical thick disk (Carollo et al. 2010). That is, at larger distances from the plane and at lower [Fe/H], the mean V_ϕ would be expected to be *lower* than it would be for a pristine thick-disk sample. We see no evidence for steepening of the gradient in Figure 7. Note that this is not to be taken as a contradiction with the Carollo et al. (2010) results, as those considered a different sample of stars, most of which were of substantially lower metallicity than those considered in the present study, and explored larger heights above the plane.

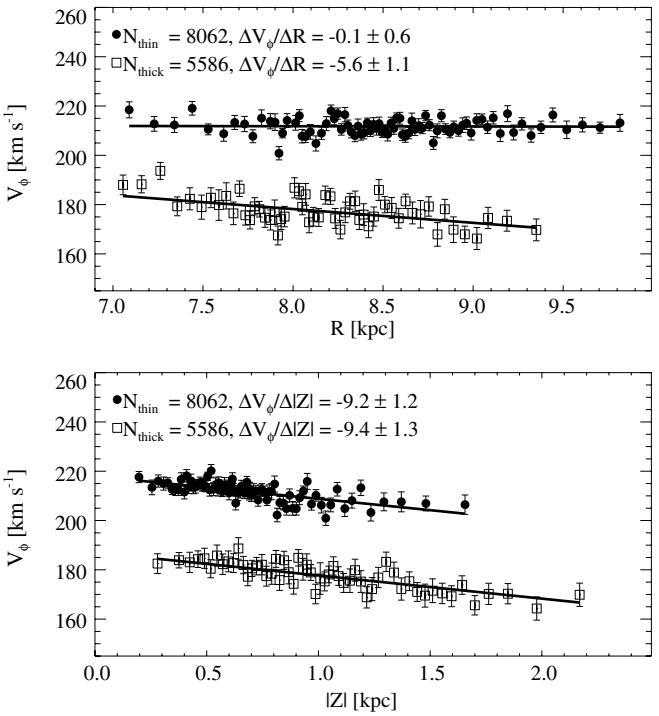

Figure 8. Rotational velocity gradients with Galactocentric radius (top panel) and with height above the Galactic plane (bottom panel), for the thin-disk (black dots) and thick-disk (open squares) subsamples. As in Figure 7, each dot represents a 3σ clipped average of 100 stars, with error bars calculated by resampling 100 stars (with replacement) 1000 times. Note that although binned data are shown for clarity, estimates of the slopes and their errors are obtained for the full unbinned data (see the text).

A gradient of about -20 to -30 km s^{-1} dex^{-1}, on average, is shown to exist for the thin-disk subsample and a strong gradient of +40 to +50 km s^{-1} dex^{-1} for the thick-disk subsample. This result for the thick-disk population agrees with the claim of Spagna et al. (2010), who derived a similar slope using F-, G-, and K-type dwarfs from SDSS DR7. However, this finding clearly contradicts the results of Ivezić et al. (2008), who found little correlation between V_ϕ and [Fe/H]. We discuss a possible resolution to this discrepancy in the Appendix.

In order to check how uncertainties in the parameters, V_ϕ, [Fe/H], [α/Fe], and $|Z|$ affect our derived gradients of V_ϕ over $|Z|$ for both the thin- and thick-disk subsamples, we have performed a simple Monte Carlo experiment. Assuming a normal distribution with width set by the 1σ estimated error for each parameter, random changes in each parameter were applied to 1000 realizations of each subsample (over the full range in $|Z|$). We obtained average gradients of -19.5 ± 1.0 km s^{-1} dex^{-1} for the thin-disk subsample and $+43.4 \pm 1.8$ km s^{-1} dex^{-1} for the thick-disk subsample, in good agreement with those shown in the bottom panel of Figure 7. We also have not found any notable correlations among the uncertainties in the parameters, which could possibly affect the derived gradients. Thus, we believe that our derived gradients of V_ϕ over [Fe/H] are not grossly affected by errors in the derived parameters.

4.2. Rotational Velocity Gradients with Distance from the Galactic Center and Galactic Plane

Figure 8 shows the overall trends of rotational velocity with distance from the Galactic center (top panel) and with vertical distance from the plane (bottom panel) for the thin-disk (black dots) and thick-disk (open squares) populations. Inspection of the top panel of this figure indicates only a negligible rotational velocity gradient for the thin-disk subsample (only -0.1 ± 0.6 km s^{-1} kpc^{-1}), consistent with a flat rotation curve in the solar neighborhood. The asymmetric drift is about 10 km s^{-1} at the solar radius, as found by previous work (e.g., Soubiran et al. 2003). A small gradient of -5.6 ± 1.1 km s^{-1} kpc^{-1} is found for the thick-disk subsample, which lags the $V_{\rm LSR}$ by $\sim$40 km s^{-1}, not far from the lag of 51 km s^{-1} obtained by Soubiran et al. (2003). Note that even if we include in the analysis the stars with 0 km s^{-1} $< V_\phi <$ 50 km s^{-1} that were eliminated in our original selection, we obtain very similar asymmetric drifts and gradients as for the case of a sample of stars that does not include them. The slopes and their uncertainties are obtained by the same way as for the gradient of V_ϕ with [Fe/H].

The bottom panel of Figure 8 shows that the gradients of V_ϕ with $|Z|$ distance are very similar (about -9.0 km s^{-1} kpc^{-1}) for both the thin- and thick-disk subsamples. The difference in V_ϕ (the velocity lag) for the high-[α/Fe] stars relative to the low-[α/Fe] stars is almost constant, $\sim$30 km s^{-1} at any given $|Z|$ distance. This again suggests that contamination from MWTD stars is not a major issue for our thick-disk subsample.

Comparing with other recent studies, the vertical gradient of V_ϕ with $|Z|$ for our thick-disk subsample, -9.4 ± 1.3 km s^{-1} kpc^{-1}, is smaller than that obtained by Casetti-Dinescu et al. (2011), -25 km s^{-1} kpc^{-1}, based on $\sim$4400 red clump metal-rich thick-disk stars covering the metallicity range $-0.6 <$ [Fe/H] $< +0.5$, that of Ivezić et al. (2008) from their SDSS sample (-29 km s^{-1} kpc^{-1}), that of Girard et al. (2006), who derived a gradient of -30 km s^{-1} kpc^{-1} from a sample of about 1200 red giants located in the range $|Z| = 1$–4 kpc, and as obtained by Chiba & Beers (2000; -30 km s^{-1} kpc^{-1}) for the subset of their non-kinematically selected stars in the metallicity range $-0.8 \leqslant$ [Fe/H] $\leqslant -0.6$ within 2 kpc of the Galactic plane. Even if we cut our thick-disk subsample to include only stars with [Fe/H] > -0.6, we obtain a slope of -7.6 ± 1.7 km s^{-1} kpc^{-1}, consistent, within 3σ, with that derived from the subsample without a metallicity restriction.

It is interesting to note that, if we consider our entire thin- and thick-disk subsamples with $|Z| > 1.0$ kpc together, we find a vertical gradient of -19.4 ± 1.8 km s^{-1} kpc^{-1}, in better agreement with the previous studies. That is, the derived vertical gradient of the rotational velocity becomes substantially steeper when the stars are not divided according to their [α/Fe] ratios. We conclude that accurate determination of the vertical gradient of V_ϕ with $|Z|$ for the thick disk *requires* application of a chemical separation criterion (other than simply [Fe/H]) to isolate the various components.

Application of our simple Monte Carlo experiment with 1000 realizations of the subsamples yielded average radial gradients of V_ϕ with R of $+0.1 \pm 0.4$ km s^{-1} kpc^{-1} and -3.7 ± 0.7 km s^{-1} kpc^{-1}, and vertical gradients with $|Z|$ of -9.2 ± 0.9 km s^{-1} kpc^{-1} and -8.2 ± 0.9 km s^{-1} kpc^{-1} for the thin- and thick-disk subsamples, respectively, without any notable covariances between the errors in the parameters involved. These values are very close to those listed in Figure 8.

4.3. Correlations of Stellar Orbital Eccentricities with Metallicity, Distance from the Galactic Center, and Height Above the Galactic Plane

Figure 9 shows trends of orbital eccentricities (e) for the G-dwarf sample, as a function of [Fe/H], R, and $|Z|$, from the top to bottom panel, respectively. The black dots denote our

Table 1
Summary of Observed Gradients for the Thin- and Thick-disk Subsamples

Correlation	$\Delta V_\phi/\Delta$[Fe/H] (km s^{-1} dex^{-1})	$\Delta V_\phi/\Delta R$ (km s^{-1} kpc^{-1})	$\Delta V_\phi/\Delta\|Z\|$ (km s^{-1} kpc^{-1})	$\Delta e/\Delta$[Fe/H] (dex^{-1})	$\Delta e/\Delta R$ (kpc^{-1})	$\Delta e/\Delta\|Z\|$ (kpc^{-1})
Thin	-22.6 ± 1.6	-0.1 ± 0.6	-9.2 ± 1.2	$+0.000 \pm 0.005$	-0.003 ± 0.002	$+0.036 \pm 0.003$
Thick	$+45.8 \pm 2.9$	-5.6 ± 1.1	-9.4 ± 1.3	-0.192 ± 0.010	$+0.030 \pm 0.004$	$+0.034 \pm 0.004$

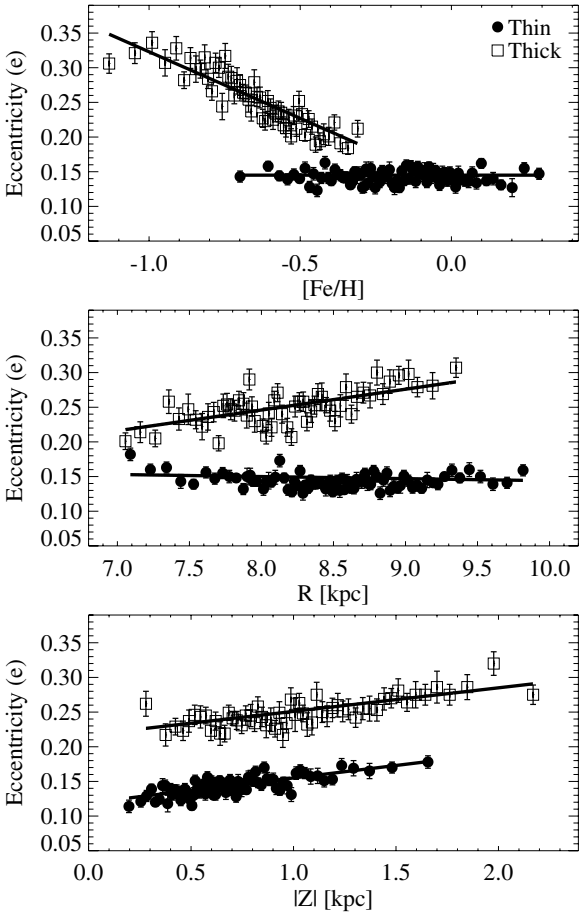

Figure 9. Trends of eccentricities as a function of [Fe/H], R, and $|Z|$, from the top to bottom panels, respectively, for the thin-disk (black dots) and thick-disk (open squares) subsamples. As in Figure 7, each dot represents a 3σ clipped average of 100 stars, with error bars calculated by resampling 100 stars (with replacement) 1000 times. Note that although binned data are shown for clarity, estimates of the slopes and their errors are obtained for the full unbinned data (see the text). The calculated gradients of e and their uncertainties are listed in Table 1.

thin-disk subsample, while the open squares indicate the thick-disk subsample.

One outstanding feature from inspection of the three panels is that the overall distribution of the orbital eccentricities for the thick-disk stars is easily separable from that for the thin-disk population. The top panel suggests that the trend of the eccentricities for the thin-disk stars is independent of metallicity, i.e., an almost flat trend of e with [Fe/H], indicative of a very narrow distribution of eccentricity, with a peak around $e \sim 0.14$. On the other hand, the trend of e for the thick-disk subsample generally increases as the metallicity decreases. A slope of -0.192 ± 0.010 dex^{-1} is obtained from a least-squares fit to the averaged points.

The second panel also shows several interesting features. As in the top panel, there is not much correlation between e and R for the thin-disk subsample, although the behavior trends slightly higher below $R = 7.5$ kpc. The thick-disk stars generally exhibit a trend of increasing e with increasing R. The eccentricity distributions for the thin- and thick-disk populations merge at $R \sim 7.0$ kpc.

The bottom panel shows that the eccentricities for both low- and high-[α/Fe] stars increase on average the farther away they are from the Galactic plane. In addition, similar to Figure 8, it is also noticed that the difference (about 0.1) in the eccentricity between the low-[α/Fe] and high-[α/Fe] subsamples is constant at any given $|Z|$.

A simple Monte Carlo experiment with 1000 realizations of the subsamples also reveals that the derived trends of the eccentricities with [Fe/H], R, and $|Z|$ above are not strongly affected by errors in the parameters involved, as the computed gradients of the eccentricities are within 3σ from those values listed in Table 1, which quantitatively summarizes various correlations discussed in this section for the two subsamples.

5. QUALITATIVE COMPARISONS WITH PREDICTIONS OF CONTEMPORARY MODELS OF DISK FORMATION

It may be unwise to rely too strongly on the present predictions of the suggested thick-disk formation models. This follows because, even though they are able to reproduce some aspects of the Milky Way's disk system, the predicted properties are limited by large uncertainties with their treatment of star formation, the dynamical interaction of presumed satellites with the disk, unavoidable numerical effects, and the myriad set of assumptions that are required in their construction. Thus, in this section, we compare our observational findings only with qualitative expectations from the published radial migration, gas-rich merger, accretion, and disk heating models. It is our expectation that, as the models and simulations improve, these comparisons will increasingly be able to discriminate between the relative importance of the various formation scenarios.

5.1. Correlations between Rotational Velocity and Metallicity

According to the radial migration models (Sellwood & Binney 2002; Roškar et al. 2008b; Schönrich & Binney 2009a; Minchev & Famaey 2010), the (presumably) metal-poor stars of the thin disk (which include young, low-[α/Fe] stars) that were born in the outer disk move inward to the solar neighborhood, whereas the (presumably) metal-rich stars that formed in the inner disk migrate outward into the solar neighborhood (as the inner region of the disk has a higher stellar and gas density, and is rapidly chemically enriched, most of the stars should be metal rich).

Schönrich & Binney (2009a) suggested that this radial movement can occur by two mechanisms: "blurring" and "churning." Blurring refers to the increase of eccentricities over time at a similar angular momentum due to scattering, e.g., on giant molecular clouds. Churning is mostly triggered by resonant scattering at co-rotation due to transient spiral density waves, which transfers stars from inner (or outer) disk regions into the solar

vicinity by changing their angular momenta without alteration of their orbital circularity (hence eccentricities). These authors suggested that churning is the dominant process by which stars in the inner disk migrate out to the solar annulus, thus providing greater heterogeneity in the abundance and velocity distributions among solar neighborhood stars.

The consequence of incomplete mixing from blurring and churning is that the metal-rich stars in the thin disk possess relatively lower rotational velocities (V_ϕ), whereas the metal-poor stars have higher V_ϕ. Thus, the expectation is that there should exist a trend of V_ϕ with [Fe/H] among (at least) the thin-disk stars. Schönrich & Binney (2009a, 2009b) indeed predicted a significant downtrend of V_ϕ with [Fe/H] for the low-[α/Fe] stars, due to incomplete mixing for younger stars. This prediction was confirmed by the later *N*-body models of Loebman et al. (2011), who employed slightly different treatments of radial mixing and star formation in their simulated disks from Schönrich & Binney (2009a, 2009b), but found a gradient of -19.7 km s^{-1} dex^{-1} for younger stars (identified with the thin-disk component with low [α/Fe]) in the solar neighborhood (7 kpc $< R <$ 9 kpc and 0.5 kpc $< |Z| <$ 1 kpc).

Our observed gradient of V_ϕ with [Fe/H] for the thin-disk stars in the range 0.5 kpc $< |Z| <$ 1.0 kpc (-23.5 ± 1.9 km s^{-1} dex^{-1}) is not far from the estimate of -20 km s^{-1} dex^{-1} obtained by Loebman et al. (2011) for their simulated sample of young, low-[α/Fe] stars in their *transition zone*, which covers the same interval in height above the plane. Note that the scale of their [α/Fe] determinations and ours are slightly different, and they also employed the predicted oxygen abundance ratio as a proxy for [α/Fe], rather than the averages employed in our estimates. It appears that an overall velocity gradient of -20 to -30 km s^{-1} dex^{-1}with metallicity for the thin-disk subsample qualitatively agrees well with the expectations from the radial migration models.

The extended tail of low-[α/Fe] metal-poor stars observed in Figures 1, 2, 4, and 5 can be also explained by the radial migration scenario. Roškar et al. (2008a) found that their simulated disk stars (when allowed to mix radially) exhibited an MDF more like the observations by Holmberg et al. (2007) than that obtained from an in situ sample without radial migration. These authors concluded that radial migration was the likely cause of the broader MDF, which is also supported by our present data.

It is noteworthy that our observed negative gradient of V_ϕ with [Fe/H] for the thin-disk stars (-20 to -30 km s^{-1} dex^{-1}) stands in contradiction to expectations from traditional local evolution models in the solar neighborhood (without allowing for mixing or migration of stars), which predict a *positive slope* of V_ϕ with [Fe/H]. According to these models, the stars that were born early in the history of star formation in the thin disk are expected to be relatively metal-poor. These old metal-poor thin-disk stars should have experienced more perturbations, such as from variations in the Galactic potential over time. As a result, such stars are expected to exhibit slower rotational velocities and larger velocity dispersions than the younger, more metal-rich thin-disk stars. This inevitably leads to the expected production of a positive gradient of V_ϕ with [Fe/H], which we clearly do not find.

When considering the radial migration models for the thick disk the case differs somewhat, in particular due to the much older ages of these stars. According to these models, it is expected that most of the thick-disk stars that exist in the solar neighborhood today were born with high velocity dispersion in the inner portion of the Galaxy, in regions of higher local density, at a time when the metallicity of the interstellar medium was relatively low and the α-abundance ratios were high. As they migrated outward over time, the lower gravitational restoring force of the local disk allowed these stars to explore orbits reaching higher above or below the plane. Relatively few thick-disk stars are thought to have migrated inward from the outer disk region. These old stars had more time to experience mixing of their orbits; in the case of complete mixing for these older stars, one might expect little or no trends between rotational velocity and metallicity.

Schönrich & Binney (2009a, 2009b) did not make predictions of velocity trends with metallicity, on the grounds that insufficient knowledge of the earliest phases of disk formation exists to constrain expectations for such a potential gradient (i.e., unknown initial conditions). However, Loebman et al. (2011) reported from their simulation an insignificant gradient of $+1.4$ km s^{-1} dex^{-1} for these older stars (>7 Gyr, which generally matched the observed properties of the thick-disk component, e.g., high [α/Fe] ratios). Even though the migration strength in their simulation induced substantial mixing, the process was still incomplete. Thus, it would allow for the conservation of significant velocity/metallicity trends. It should be mentioned, however, that their model was not specifically intended to match the properties of the Milky Way.

In any case, the small or absent predicted correlations between V_ϕ and [Fe/H] for the high-[α/Fe] stars from the migration models are in contrast to our determination of a steep gradient of +40 to +50 km s^{-1} dex^{-1} for the observed high-[α/Fe] stars we associate with the thick disk, as shown in Figure 7. Thus, this trend of V_ϕ with [Fe/H] for the thick-disk subsample can provide a useful constraint to the radial migration models mentioned above.

In summary, the observed correlations between V_ϕ and [Fe/H] for our low-[α/Fe] (thin-disk) stars can be naturally explained by the radial migration of stars from the outer disk (more metal-poor stars) and from the inner disk (more metal-rich stars) into the solar vicinity, as predicted by the migration models. As explained by Schönrich & Binney (2009b), such a velocity gradient arises from the interplay between the churning and the blurring processes. The behavior of the high-[α/Fe] (thick-disk) stars is rather different (exhibiting a much steeper gradient) than that expected from the simulated high-[α/Fe] stars of Loebman et al. (2011), although there remains the uncertainty of how well thick-disk stars are represented in these models, and how well the models match the actual history of the Milky Way. It appears that stellar radial migration may have played an important role in the evolution of the thin disk, but, based on the information available from the current radial migration models and simulations, it is difficult to ascertain the relative importance of radial migration for the formation and/or evolution of the thick disk.

5.2. Rotational Velocity Gradients with Distance from the Galactic Center and Galactic Plane

The gas-rich merger model of Brook et al. (2007) predicts a correlation between V_ϕ and R for stars in the disk system. According to their simulations (especially their Figure 5) there should exist a detectable velocity gradient for the thin disk in the region of the solar neighborhood (R = 7–10 kpc). This differs from our null gradient for the thin-disk subsample. Their simulations also indicate a negligible gradient for their

thick-disk stars (which they refer to as "merger stars"), which is at least qualitatively in line with our small value of -5.6 ± 1.1 km s^{-1} kpc^{-1}. However, it should be kept in mind that, as Richard et al. (2010) demonstrated in their various gas-rich merger simulations, the initial orbital parameters of the mergers strongly affect the final kinematics and structures of the resulting disk populations. Brook et al. (2007) performed a simulation with a particular set of parameters to produce their disk systems, which may not necessarily match those of the Galaxy. For example, one rather large difference between this particular simulation and our results is that, while we find a difference in velocity lag of about 30 km s^{-1} between our thin and thick-disk subsamples, the *N*-body prediction calls for a difference of over 150 km s^{-1}. Additional simulations of this process, better matched to the nature of the Milky Way, would clearly be useful for comparison with our results.

The dynamical heating of a pre-existing thin disk, as modeled by the simulations from Villalobos et al. (2010), also predicts gradients of V_ϕ with respect to both R and $|Z|$. Looking at their Figure 14, the thickened-disk component exhibits a very weak trend of V_ϕ with R for low initial orbital inclination of the merging satellite, while the correlation between the two quantities becomes stronger as the incidence angle is increased. Concerning the gradient of V_ϕ with $|Z|$, it is evident in their Figure 14 that the vertical gradient of V_ϕ is much shallower at higher orbital inclination. Thus, roughly speaking, our radial gradient of V_ϕ for the thick-disk subsample agrees better with that expected for low orbital inclination of the merging satellite, but our vertical gradient is better matched by mergers with high orbital inclination. This may indicate that the compromise case of intermediate orbital inclination ($i = 30°$) best describes our observed results, a possibility also considered by Villalobos et al. (2010). In any event, the comparisons of our thick-disk subsample with this particular model prediction imply that if the heating scenario played a major role in the formation of the thick disk, the initial orbital inclination of the merging satellite could not have been too small or too large. Of course, it is also possible that multiple satellite mergers may have been involved, which complicates these simple comparisons with a single merger.

In summary, comparisons of our data with the gas-rich merger model from Brook et al. (2007) suggest that, while this model may not explain the lack of a rotational velocity gradient with Galactocentric distance for the thin disk, it does account for that which is observed for the thick disk. However, the much larger difference in the velocity lag than our finding between the thin- and thick-disk stars remains to be resolved. The model of thin-disk heating by mergers of Villalobos et al. (2010) qualitatively agrees with the expected kinematic features of our thick-disk subsample, assuming that the merging satellite has an intermediate orbital inclination.

In the previous section, which considered correlations between V_ϕ and [Fe/H], our results for the thin-disk population were shown to be in qualitative accord with predictions of the radial migration models, whereas those for our thick-disk population might not be. In order to be confident of the implications of this result, one would like to compare it with the predictions from more refined radial migration models that better reproduce the observed properties of the thick-disk population. On the other hand, the relationship between V_ϕ with R and $|Z|$ for the high-[α/Fe] stars agrees better with the predictions of the gas-rich merger and thin-disk heating models that we have considered here. Taken as a whole, the presently available comparisons of the various observed gradients suggest that the thick disk may have formed from either the mergers of gas-rich systems or the heating of a pre-existing thin disk by mergers, and has been little influenced by the secular process of stellar migration, whereas radial migration may well have strongly affected the evolution of the thin disk.

5.3. Distribution of Stellar Orbital Eccentricities

Sales et al. (2009) demonstrated that the orbital eccentricities of a stellar population could also be used as a tool to probe the formation and evolution mechanisms of the disk system. In particular, taken at face value (and recognizing that their summary only pertains to a limited set of model parameters and histories), their Figure 3 suggests that radial migration models (e.g., Roškar et al. 2008b) generate symmetric distributions of stellar eccentricities with rather narrow widths, whereas the gas-rich merger models (e.g., Brook et al. 2004, 2005) produce distributions that are skewed toward higher eccentricity with larger widths. The accretion models (e.g., Abadi et al. 2003) distribute the eccentricities rather broadly over a wide range. For the disk heating scenario (e.g., Villalobos & Helmi 2008), there is a similarity of the eccentricity distribution with that of the merger model for $e < 0.6$, but there exists a secondary peak at high eccentricity ($e \sim 0.8$). Generally, they found that violent models such as disk heating and accretion generated a distribution of stellar orbital eccentricities spanning a large range, with secondary peaks at higher eccentricity, or at least with rather broad distributions of high eccentricity stars. By contrast, the smooth transition models such as radial migration or in situ star formation from gas-rich mergers produced distributions dominated by lower eccentricity orbits covering relatively narrower ranges.

Several studies have compared the above expectations from these models to observed distributions of orbital eccentricities for thick-disk stars in the solar neighborhood. Wilson et al. (2011), for example, investigated the eccentricity distribution of a sample of thick-disk stars from RAVE. They concluded that their observed distribution, which peaked at low eccentricity and exhibited a lack of high eccentricity stars, disfavored the pure accretion model of Abadi et al. (2003), and was most consistent with the predictions of gas-rich merger models. Dierickx et al. (2010) carried out a similar test, using a large sample of dwarfs from SDSS DR7, and suggested that their sample favored the gas-rich merger scenario as well. Casetti-Dinescu et al. (2011) performed an analysis using a sample of ~4400 red clump thick-disk stars from RAVE Data Release 2 (Zwitter et al. 2008) with available proper motions from SPM4. Their comparison of the derived orbital eccentricity distribution with model predictions supported the gas-rich merger scenario or possibly the minor merger heating model (arguing that the expected secondary peak at high eccentricity could be avoided, depending on the initial orbital configuration of the merging satellite(s)). Indeed, a recent simulation study by Di Matteo et al. (2011) showed that, with the adoption of a particular set of initial conditions (a 1:10 mass ratio and direct orbit of a presumed single interacting satellite), the disk heating model could also produce the distribution of eccentricities observed by Wilson et al. (2011) and Dierickx et al. (2010) *without* creating a secondary peak at high eccentricity, confirming that the heating model may also be a viable mechanism for thick-disk formation.

It is noteworthy that the various observational studies, based on different samples, with different distance estimates, and adopting different models for the Milky Way potential, all

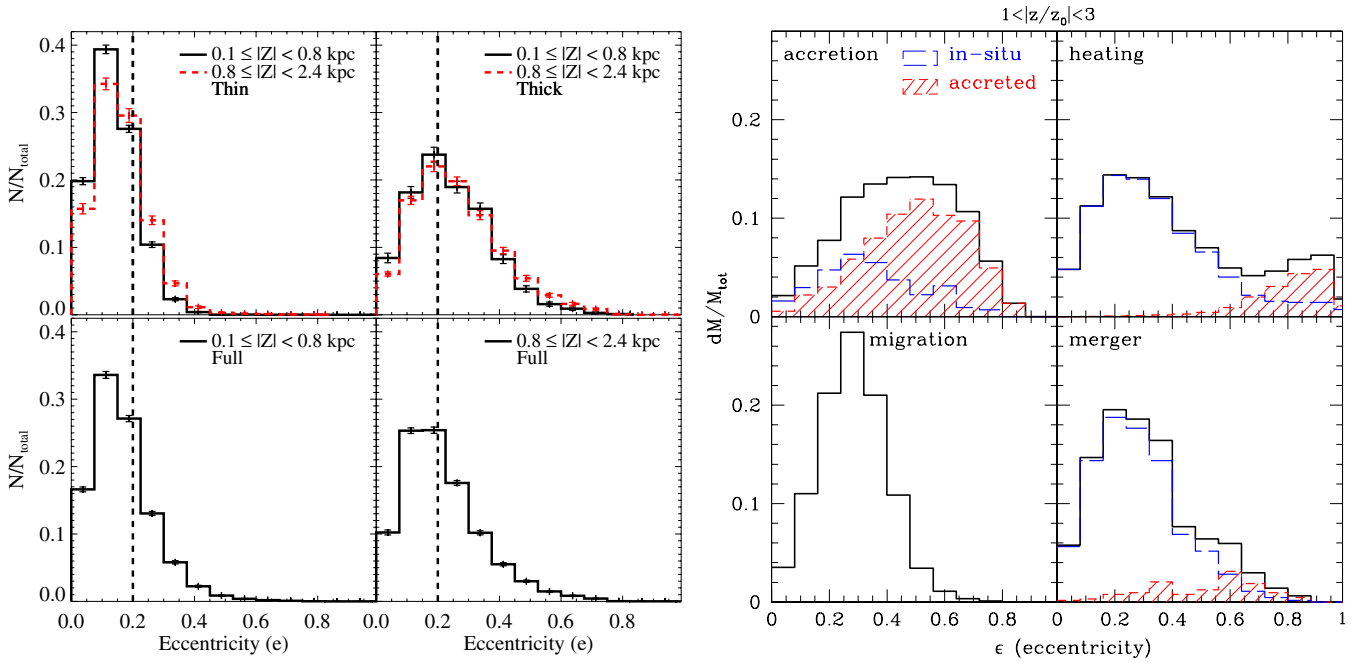

Figure 10. Left panel: normalized distributions of eccentricities for the low-[α/Fe] stars (top left panel), high-[α/Fe] stars (top right panel), and for the entire G-dwarf sample (two bottom panels) over different $|Z|$ ranges. The vertical dashed line provides a reference at $e = 0.2$. The error bars are calculated by drawing from the sample with replacement 1000 times. A typical error in e is 0.044. Right panel: a reproduction of Figure 3 from Sales et al. (2009). The formation scenarios depicted are adopted from Abadi et al. (2003) for the accretion model, Villalobos & Helmi (2008) for the heating model, Roškar et al. (2008a) for the radial migration model, and Brook et al. (2004, 2005) for the gas-rich merger model. We adopt a bin size of 0.075 in the left-hand panels, close to that used in the Sales et al. figure. Taking the scale height (Z_0) of the thick disk as 0.8 kpc, the range $1 < |Z/Z_0| < 3$ in the Sales et al. figure corresponds to the range 0.8 kpc $< |Z| <$ 2.4 kpc.

produce similar eccentricity distributions for the thick-disk population—a broad peak at low eccentricity and a lack of high eccentricity stars. Considering all of the studies mentioned above, the favored mechanisms for thick-disk formation are likely to be either (or both) the gas-rich mergers model or the thin-disk heating by minor mergers scenario, at least when considering only stellar orbital eccentricities as a probe. All of these studies rejected the pure accretion model of thick-disk formation (as advocated by Abadi et al. 2003).

Unlike the previous observational studies mentioned above, which selected thick-disk stars mostly on the basis of spatial extent, we have selected a subsample of likely thick-disk stars based on their measured [α/Fe], as described in Section 3. We now compare the eccentricity distribution of our thick-disk subsample with expectations from each model cited in Sales et al. (2009). The left-hand set of panels of Figure 10 displays the normalized distributions of eccentricity for the low-[α/Fe] (top left) and high-[α/Fe] (top right) populations. Each distribution in the top two panels is restricted to different slices on distance from the Galactic plane, as listed in the figure legend. The e distribution of the entire G-dwarf sample (without splits based on [α/Fe]), divided into regions that should emphasize the thin- and thick-disk regions, is shown in the bottom left and bottom right panels, respectively.

The eccentricity distributions of the thin-disk subsample peak at much less than $e = 0.2$, with narrow widths, and apparently include very few high eccentricity stars ($e > 0.4$) for the two $|Z|$ regions shown in the top left panel. In contrast, the distributions for the thick-disk subsample shown in the top right panel peak at $e \sim 0.2$ and exhibit extended tails of higher eccentricities up to $e \sim 0.8$; there remains a relative lack of high eccentricity stars ($e > 0.6$). Although we find that the relative frequency of the high-e stars slightly increases at larger $|Z|$ distance (red dashed line) for both subsamples, the distributions otherwise do not change significantly. This again confirms that the population separation based on [α/Fe] appears to work quite well. The eccentricity distributions for the full sample of G-dwarf stars exhibit some rather interesting features. Even at large $|Z|$ distance (0.8–2.4 kpc, bottom right), where the thick-disk stars should dominate, the eccentricity *does not appear similar* to that of the thick-disk subsample separated by [α/Fe] (top right panel) in either range of $|Z|$ distance; the peak and the width do not match. This underscores once more that, for the purpose of the selection of thick-disk stellar samples, purely spatial separations are insufficient.

Comparing with the published model predictions in Sales et al. (2009), as shown in the right-hand panels of Figure 10, the relative shortage of high eccentricity stars and the absence of the secondary peak at high $e \sim 0.8$ in our observed distribution exclude the accretion origin and the disk heating model for the thick disk. Although the distribution expected from the radial migration models provides a viable description of stars in the low eccentricity region, it fails to capture the observed high eccentricity tail of the thick-disk stars. The skewed distribution of observed eccentricities toward higher values is not well represented by the radial migration predictions, which exhibit a more Gaussian-like shape (lower left panel of the right-hand panels of Figure 10). It should be noted, however, that an alternative radial migration model by Schönrich & Binney (2009a, 2009b) indicates the presence of a peak eccentricity between 0.1 and 0.2, with an extended tail toward high eccentricities, which is consistent with the shape of the observed e distribution of our thick-disk sample. Hence, we must be cautious in drawing firm conclusions on the formation mechanisms of the thick disk due to their apparent sensitivity to details of the models and simulations. Solely based on comparisons with the predictions in the published models from Sales et al. (2009), it seems that our eccentricity distribution

most closely resembles that predicted from the gas-rich merger scenario.

The eccentricity distribution of our thick-disk subsample differs little from the disk heating model of the Di Matteo et al. (2011) simulation. As identified by this simulation (and also mentioned in the discussions of the observations of Casetti-Dinescu et al. 2011 and Wilson et al. 2011), the secondary peak or high eccentricity region ($e > 0.6$) in the disk heating model is mostly occupied by the accreted stars (which retain the initial orbital characteristics of the merging satellite). In addition, depending on the initial conditions (especially the orbital inclination of the interacting satellite) of the simulation, the high eccentricity secondary peak may (or may not) be seen in the predicted distribution of the eccentricities. In particular, the small satellite mass (1:10 mass ratio) in the Di Matteo et al. simulation would likely not contribute large numbers of stars to the solar neighborhood.

It appears from our observed eccentricity distribution, and that of others, that the inclination of the merging small galaxy in the simulation of the disk heating model in Sales et al. (2009) may be less than 30°. This is qualitatively consistent with the findings from the correlations of V_ϕ with R and $|Z|$ in the previous section. We stress that the existence of the secondary peak at high eccentricity and clear identification of the extended tail of the high eccentricity with observational data can provide strong constraints on the initial conditions on the merger or heating models.

The observed eccentricity distribution of the full G-dwarf sample at larger distances from the Galactic plane, or for the thick-disk population with high-[α/Fe] ratios, rule out a broad peak at intermediate eccentricity. This argues strongly against the importance of an accretion origin of the thick-disk component, unless the accretion model can explain the dominant population in the low eccentricity regime. At this stage, confident distinction between the other published models is infeasible because uncertainties in the initial conditions, in the N-body simulations themselves (e.g., artificial heating), and in the assumed model parameters (potential, secular heating, star formation histories, etc.) can produce differences that are roughly comparable to the predicted differences *between* various scenarios.

6. SUMMARY AND CONCLUSIONS

We have assembled a sample of ∼17,300 G-type dwarfs with available low-resolution ($R \sim 2000$) spectroscopy from SEGUE, a sub-survey conducted during SDSS-II. The sample we considered comprises stars with $d < 3$ kpc, $\log g \geqslant 4.2$, spectra having S/N $\geqslant 30$ Å^{-1}, $V_\phi > +50$ km s^{-1}, [Fe/H] > -1.2, and 7 kpc $< R <$ 10 kpc. A separate test was carried out to eliminate a small number of stars that had larger probability of being associated with the halo than the disk system.

Unlike the conventional assignment of stars into thin- and thick-disk components based on kinematics (or spatial distribution), we have made use of [α/Fe] as a reference to *chemically divide* our G-dwarf sample into likely thin-disk and thick-disk populations.

Our chemically separated populations indicate that a negative rotational velocity gradient with increasing [Fe/H] exists for the thin-disk population (-22.6 ± 1.6 km s^{-1} dex^{-1}), whereas the thick-disk population exhibits a positive slope ($+45.8 \pm 2.9$ km s^{-1} dex^{-1}) in the range 0.1 kpc $< |Z| <$ 3.0 kpc and $R = 7$–10 kpc. Larger mean orbital radii are also noticed among the metal-poor thin-disk stars, as compared with the more metal-rich thin-disk stars, and smaller mean orbital radii are found for the thick-disk stars compared with the thin-disk stars.

Table 2
Results of Qualitative Comparison Tests with Predictions of Published Models for Thick-disk Formation

Model	$\Delta V_\phi/\Delta$[Fe/H]	$\Delta V_\phi/\Delta R$	$\Delta V_\phi/\Delta\|Z\|$	e Distribution
Accretion	N/A	N/A	N/A	Failed
Disk heating	N/A	Passed	Passed	Failed
Radial migration	Indecisive[a]	N/A	N/A	Indecisive
Gas-rich mergers	N/A	Passed	N/A	Passed

Notes. N/A indicates that a model prediction is not available. The adopted thick-disk formation models are drawn from Abadi et al. (2003) for the accretion model, Villalobos & Helmi (2008) for the heating model, Roškar et al. (2008a) for the radial migration model, and Brook et al. (2004, 2005) for the gas-rich mergers model.
[a] Based on the comparisons with predictions by Schönrich & Binney (2009a, 2009b) and Loebman et al. (2011).

The distribution of rotational velocity appears independent of R for our thin-disk subsample, while there exists a very small correlation (-5.6 ± 1.1 km s^{-1} kpc^{-1}) between V_ϕ and R for our thick-disk subsample.

We have found that the observed lag of V_ϕ for the high-[α/Fe] stars relative to the low-[α/Fe] population is quite constant at a given $|Z|$ distance (30 km s^{-1}), implying that our chemically separated populations are indeed distinct components in terms of their kinematics. This also allows us to infer that division by chemistry reveals the kinematic structure of each population better than division on the basis of spatial separation.

The vertical gradient of V_ϕ with $|Z|$ for our thick-disk subsample (-9.4 ± 1.3 km s^{-1} kpc^{-1}) is smaller than that reported by Casetti-Dinescu et al. (2011; -25 km s^{-1} kpc^{-1}), Ivezić et al. (2008; -29 km s^{-1} kpc^{-1}), Girard et al. (2006; -30 km s^{-1} kpc^{-1}), and Chiba & Beers (2000; -30 km s^{-1} kpc^{-1}). Without application of our proposed separation of the thin- and thick-disk subsamples, we find a vertical gradient of -19.4 ± 1.8 km s^{-1} kpc^{-1} for the stars with $|Z| > 1.0$ kpc, in better agreement with the previous observational studies. Hence, depending on how the thick-disk stars are selected (spatially or chemically), the kinematic trends change. Assuming that the thick disk is a distinct component comprised of stars with high-[α/Fe] ratios, we again stress that the chemical separation of the thick disk provides a more clear picture of the kinematics.

It appears that there is no correlation between orbital eccentricity and metallicity for the thin-disk subsample, whereas the trend of e for the thick-disk subsample rather steeply increases as the metallicity decreases. The e distribution for the low-[α/Fe] stars appears to be independent of R, whereas the high-[α/Fe] stars exhibit an increasing trend with distance from the Galactic center. The difference in average orbital eccentricity between the low-[α/Fe] and high-[α/Fe] subsamples appears constant at any given $|Z|$ (about 0.1), which also indicates a clear distinction between these populations. Our approach of separating the thin-disk and thick-disk components by chemical tagging on their [α/Fe] abundance ratios yields well-defined, and distinct, kinematic trends for these populations as listed in Table 1.

The rotational velocity gradient for the thin-disk subsample with metallicity qualitatively agrees with the predictions of the radial migration models (Schönrich & Binney 2009b; Loebman et al. 2011). Table 2 summarizes the results of qualitative

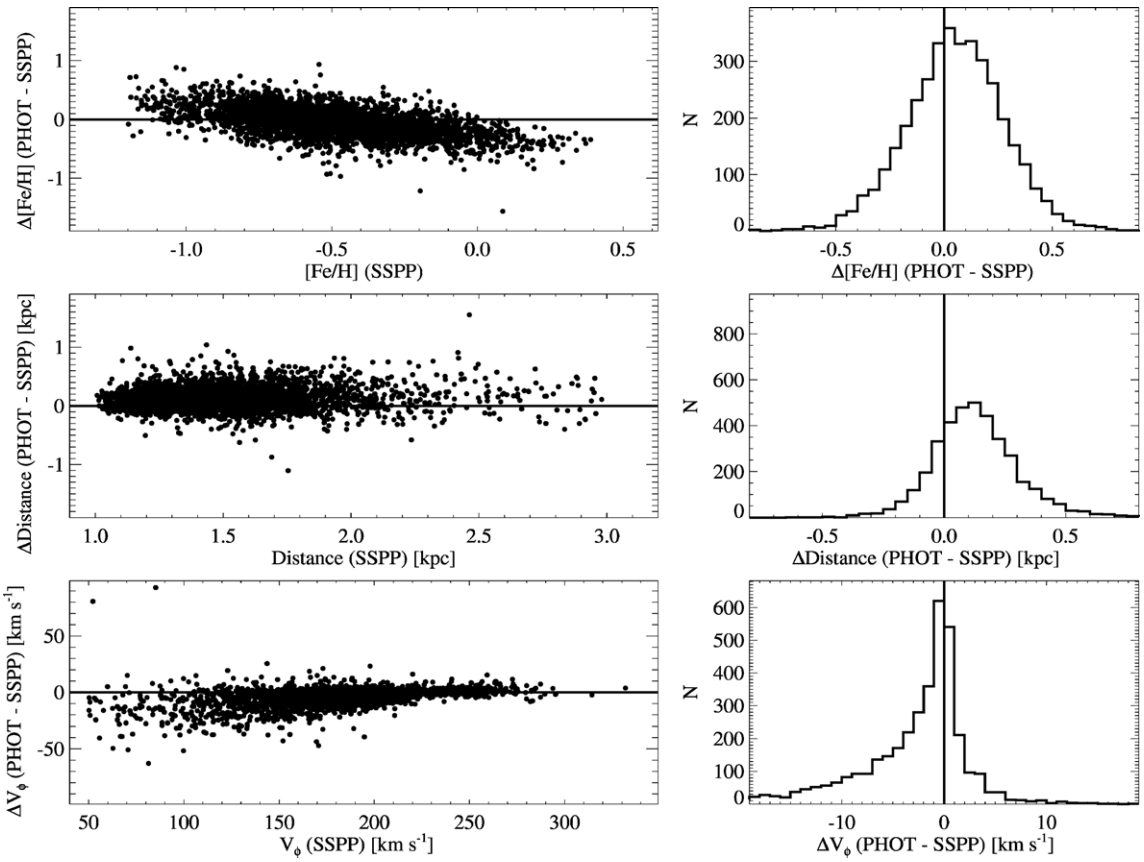

Figure 11. Scatter plots (left panels) and histograms (right panels) of the differences in [Fe/H], distance, and V_ϕ, from top to bottom, between the photometric estimates (PHOT) and our estimates (SSPP; see the text for details of the determination of the "PHOT" parameters).

comparisons of the various thick-disk formation scenarios with the observed properties of our G-dwarf sample, based on predictions from these published (but still rather primitive) models.

Based on these results, radial migration appears to have influenced the structural and chemical evolution of the thin disk, but may not have played a prominent role in the formation and evolution of the thick disk. However, to be certain of this inference, comparisons with the predictions of more refined radial migration models that better reproduce the observed properties of the thick-disk population of the Milky Way galaxy are required. The preponderance of evidence, based on qualitative comparisons with existing thick-disk formation models, indicates that the thick disk of the Milky Way may have resulted from gas-rich mergers or from heating of a pre-existing thin disk by minor mergers. We again emphasize that, although all of the models considered have had some success in reproducing aspects of the thick disk, no one theory has emerged that fully accounts for its detailed observed properties. We expect that newer generation models and simulations will be strongly constrained by observations such as those presented here.

Funding for SDSS-I and SDSS-II has been provided by the Alfred P. Sloan Foundation, the Participating Institutions, the National Science Foundation, the U.S. Department of Energy, the National Aeronautics and Space Administration, the Japanese Monbukagakusho, the Max Planck Society, and the Higher Education Funding Council for England. The SDSS Web site is http://www.sdss.org/.

This work was supported in part by grants PHY 02-16783 and PHY 08-22648: Physics Frontiers Center/Joint Institute for Nuclear Astrophysics (JINA), awarded by the U.S. National Science Foundation. J.A.J. acknowledges support from NSF grant AST-0607482. Ž.I. acknowledges support from NSF grants AST 06-15991 and AST-07 07901, as well as from grant AST 05-51161 to LSST for design and development activities. A.J. acknowledges support from DFG grant SFB 881. R.S. acknowledges financial and material support from Max-Planck-Gesellschaft. H.L.M. acknowledges support from NSF grant AST-1009886. D.A. acknowledges support from the Ewha Womans University Research Grant of 2010, as well as support by the National Research Foundation of Korea to the Center for Galaxy Evolution Research.

Note added in proof. Some of the cited values in our paper from the work of Loebman et al. are from the preprint version (posted in 2010) of their work (Loebman et al. 2011) and are slightly different in the published version. The published version also added some new results that are very relevant to ours. We summarize these below.

Loebman et al. (2011) newly derived a rotational gradient of -24.8 km^{-1} s^{-1} dex^{-1} with [Fe/H] for their low-[α/Fe] stars, and $+13.5$ km^{-1} s^{-1} dex^{-1} for their high-[α/Fe] stars, which are slightly different than our cited values of -19.7 km^{-1} s^{-1} dex^{-1} and $+1.4$ km^{-1} s^{-1} dex^{-1}, respectively. These new values are even closer to our derived gradients, and our interpretations do not change.

Loebman et al. (2011) also added an estimate of the rotational velocity gradient with distance from the Galactic plane for high- and low-[α/Fe] stars. As these results can be directly

compared with ours in the bottom panel of our Figure 8, we summarize their results here.

Loebman et al. (2011) found a vertical gradient of -9 km^{-1} s^{-1} kpc^{-1} for their low-[α/Fe] stars and -11 km^{-1} s^{-1} kpc^{-1} for their high-[α/Fe] stars in the range $R = 7$ to 9 kpc. These gradients are in a good agreement with our estimate of about -9 km^{-1} s^{-1} kpc^{-1} for both subsamples. Interestingly, when considering the overall sample, their derived gradient of -18 km^{-1} s^{-1} kpc^{-1} is also very close to our value of -21.9 ± 0.8 km^{-1} s^{-1} kpc^{-1} for our entire sample. In addition, the velocity shift of our high-[α/Fe] stars, relative to the low-[α/Fe] stars, is about 30 km^{-1} s^{-1}, while their Figure 16 indicates a velocity lag of about 20 km^{-1} s^{-1} for their simulated stars, which is not far from ours. Based on these results, it appears that radial migration may play more of a role in structuring the presently observed thick disk, because the radial migration model they employ apparently mimics the observed properties from our sample in terms of the velocity gradient with distance from the Galactic plane. In Table 2, we would change "N/A" to "Passed" in the fourth column for the radial migration model.

However, as seen from the comparisons of the velocity gradient with metallicity for the thick-disk subsample, it remains to be resolved why the predicted velocity gradient with metallicity is less steep, and also why the velocity lag is smaller than ours. Clearly, what is required are better and more physically realistic radial migration models and simulations in order to confirm the observed characteristics; our results provide vital constraints to which these can be compared.

APPENDIX

RESOLVING OBSERVATIONAL CONFLICTS ON CORRELATIONS BETWEEN ROTATIONAL VELOCITY AND METALLICITY

The recent study of Ivezić et al. (2008) concluded, on the basis of their analysis of a complete photometric sample from SDSS, that there existed little or no correlation between V_ϕ and [Fe/H] for stars in the disk system of the Milky Way, a finding confirmed by Bond et al. (2010). However, based on a spectroscopic sample of dwarfs from SDSS DR7, Spagna et al. (2010) reported a gradient of 40–50 km s^{-1} dex^{-1} for stars with $-1.0 <$ [Fe/H] < -0.5 and 1 kpc $< |Z| <$ 3 kpc. Loebman et al. (2011) claimed that the gradient found by Spagna et al. (2010) was caused by selection bias in the SDSS spectroscopic sample. As our current analysis also reveals a trend of V_ϕ with [Fe/H] for likely thick-disk stars, of similar size to that reported by Spagna et al., we have attempted to resolve these contradictory results between the various studies.

As a first step, we employ the relationship devised by Ivezić et al. (2008) to obtain absolute magnitudes in the r band, and derive distances for our G-dwarf sample that should be on the same scale as theirs. Their adopted relationship is

$$M_r(g-i,\mathrm{[Fe/H]}) = -0.56 + 14.32\,x - 12.97\,x^2 + 6.127\,x^3 - 1.267\,x^4 + 0.0967\,x^5 - 1.11\,\mathrm{[Fe/H]} - 0.18\,\mathrm{[Fe/H]}^2, \quad \text{(A1)}$$

where $x = (g - i)$. The above is the combined relationship of Equations (A2), (A3), and (A7) in Ivezić et al. (2008). Then, by adopting the improved expression by Bond et al. (2010), we estimate the photometric metallicities for our sample. The adopted relationship is as follows:

$$\mathrm{[Fe/H]_{PHOT}} = -13.13 + 14.09\,x + 28.04\,y - 5.51\,xy - 5.90\,x^2 - 58.68\,y^2 + 9.14\,x^2y - 20.61\,xy^2 + 0.00\,x^3 + 58.20\,y^3, \quad \text{(A2)}$$

where $x = (u - g)$ and $y = (g - r)$. All colors are reddening corrected, and note that the coefficient of the x^3 term is zero. We refer to the distance determined with Equation (A1) as the "photometric distance," the metallicity estimated by Equation (A2) as the "photometric metallicity," and the rotation velocity calculated using the photometric distance in combination with the measured radial velocities and proper motions as the "photometric rotational velocity." The label "PHOT" in Figures 11 and 12 indicate these estimates, while the label "SSPP" denotes the values we have used for the G-dwarf sample.

Figure 11 shows scatter plots (left panels) and histograms (right panels) of the differences in [Fe/H], distance, and V_ϕ between the photometric (PHOT) estimates and our estimates (SSPP) for stars in $|Z| = 1.0$–1.5 kpc from our G-dwarf sample considered in this paper. It can be noticed from inspection of the top panels that the photometric metallicity is consistently higher at low [Fe/H] and lower at high [Fe/H], compared with the SSPP estimates, with an overall shift of about 0.1 dex (top right panel).

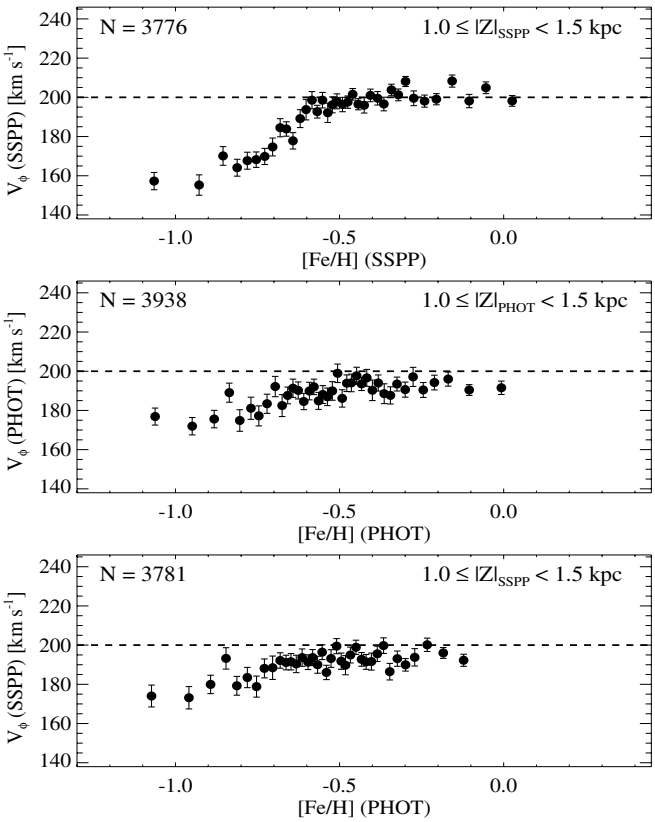

Figure 12. Derived rotational velocity gradients as a function of metallicity. The top panel shows the trend with the SSPP-derived quantities for all stars at $|Z| = 1.0$–1.5 kpc from our G-dwarf sample. Note that the SSPP-determined $|Z|$ distance is used to select these stars. The middle panel are the photometric determinations in the same interval of height above the plane. Note that there are more objects selected in this $|Z|$ distance range, which was calculated using Equation (A1). The bottom panel displays the trend of our values of V_ϕ vs. the photometric metallicity, and a very similar pattern between the middle and the bottom panel is observed. The error bar on each point is calculated by resampling 100 stars with replacement 1000 times.

The middle panels suggest that our distance determination is on average ∼0.1 kpc lower than the photometric estimate, with a trend that this deviation becomes larger as the distance increases. The bottom panels show that our rotational velocities generally agree with the photometric rotational velocities, but our values trend higher at low V_ϕ.

With these differences (especially for [Fe/H]) kept in mind, we have examined the trend of V_ϕ with [Fe/H] based on the photometric estimates and based on the spectroscopic estimates, for stars in the range $|Z| = 1.0$–1.5 kpc. Figure 12 shows the results. The top panel makes use of the spectroscopically derived quantities and the middle panel comes from the photometric quantities. Due to the small difference in the distance estimates (larger distances for the photometric distance), we see in the middle panel that there are more objects selected in this $|Z|$ distance range, which does not affect our conclusions. It is obvious that we obtain a flattening of the V_ϕ relationship below [Fe/H] < -0.5 for the photometrically determined values. Even if we consider the photometric metallicity and *our values* of V_ϕ, we obtain a very similar pattern (bottom panel). This strongly suggests that the effect of the input metallicity in Equation (A1) on distance for calculation of V_ϕ is minimal. However, it is clear that the difference between use of the photometric metallicity and the spectroscopic metallicity makes a large difference in the derived trend of V_ϕ. This can be accounted for by the scattering of higher metallicity stars (which have high V_ϕ) into the photometrically determined low-metallicity region, resulting in a flatter gradient of V_ϕ with [Fe/H] for stars with [Fe/H] < -0.5, as seen by comparing the middle panel of Figure 12 with the top panel.

There are at least two reasons that the photometric metallicity relation in Equation (A2) may assign the metallicity of a star to a value that strongly deviates from that estimated from the SSPP. First, Equation (A2) was not calibrated with the metallicity estimates used in this study, but with those available in DR7. There has been significant improvement in the SSPP for estimation of [Fe/H] since the DR7 release, especially for stars with near-solar and super-solar values (see Smolinski et al. 2011). For a proper comparison, the photometric metallicity relation needs to be re-calibrated with the metallicities available from the DR8 release. The other reason is that small random errors in the photometric measurements (and zero points) can strongly influence the photometric metallicity estimate (and its errors; Ž. Ivezić et al. 2011, in preparation). As a result, stars that are in reality of high metallicity can be artificially moved into the low-metallicity region.

REFERENCES

Abadi, M. G., Navarro, J. F., Steinmetz, M., & Eke, V. R. 2003, ApJ, 597, 21
Abazajian, K. N., Adelman-McCarthy, J. K., Agüeros, M. A., et al. 2009, ApJS, 182, 543
Aihara, H., Allende Prieto, C., An, D., et al. 2011, ApJS, 193, 29
Allende Prieto, C., Sivarani, T., Beers, T. C., et al. 2008, AJ, 136, 2070
An, D., Johnson, J. A., Beers, T. C., et al. 2009a, ApJ, 707, L64
An, D., Pinsonneault, M. H., Masseron, T., et al. 2009b, ApJ, 700, 523
An, D., Terndrup, D. M., Pinsonneault, M. H., et al. 2007, ApJ, 655, 233
Andrievsky, S. M., Luck, R. E., Martin, P., & Lépine, J. R. D. 2004, A&A, 413, 159
Barbanis, B., & Woltjer, L. 1967, ApJ, 150, 461
Bensby, T., Feltzing, S., & Lundström, I. 2003, A&A, 410, 527
Bensby, T., Feltzing, S., Lundström, I., & Ilyin, I. 2005, A&A, 433, 185
Bond, N. A., Ivezić, Ž., Sesar, B., et al. 2010, ApJ, 716, 1
Brook, C., Richard, S., Kawata, D., Martel, H., & Gibson, B. K. 2007, ApJ, 658, 60
Brook, C. B., Gibson, B. K., Martel, H., & Kawata, D. 2005, ApJ, 630, 298
Brook, C. B., Kawata, D., Gibson, B. K., & Freeman, K. C. 2004, ApJ, 612, 894
Carollo, D., Beers, T. C., Chiba, M., et al. 2010, ApJ, 712, 692
Casetti-Dinescu, D. I., Girard, T. M., Korchagin, V. I., & van Altena, W. F. 2011, ApJ, 728, 7
Chiba, M., & Beers, T. C. 2000, AJ, 119, 2843
Dierickx, M., Klement, R. J., Rix, H.-W., & Liu, C. 2010, ApJ, 725, L186
Di Matteo, P., Lehnert, M. D., Qu, Y., & van Driel, W. 2011, A&A, 525, L3
Fuchs, B. 2001, MNRAS, 325, 1637
Fuhrmann, K. 1998, A&A, 338, 161
Fuhrmann, K. 2008, MNRAS, 384, 173
Gilmore, G., & Reid, N. 1983, MNRAS, 202, 1025
Gilmore, G., Wyse, R. F. G., & Bryn Jones, J. 1995, AJ, 109, 3
Girard, T. M., Korchagin, V. I., Casetti-Dinescu, D. I., et al. 2006, AJ, 132, 1768
Girard, T. M., van Altena, W. F., Zacharias, N., et al. 2011, AJ, 142, 15
Haywood, M. 2001, MNRAS, 325, 1365
Haywood, M. 2008, MNRAS, 388, 1175
Holmberg, J., Nordström, B., & Andersen, J. 2007, A&A, 475, 519
Ivezić, Ž., Sesar, B., Jurić, M., et al. 2008, ApJ, 684, 287
Jenkins, A. 1992, MNRAS, 257, 620
Kazantzidis, S., Bullock, J. S., Zentner, A. R., Kravtsov, A. V., & Moustakas, L. A. 2008, ApJ, 688, 254
Lee, Y. S., Beers, T. C., Allende Prieto, C., et al. 2011, AJ, 141, 90
Lee, Y. S., Beers, T. C., Sivarani, T., et al. 2008a, AJ, 136, 2022
Lee, Y. S., Beers, T. C., Sivarani, T., et al. 2008b, AJ, 136, 2050
Lemasle, B., Francois, P., Bono, G., et al. 2007, A&A, 467, 283
Loebman, S. R., Roškar, R., Debattista, V. P., et al. 2011, ApJ, 737, 8
Magrini, L., Sestito, P., Randich, S., & Galli, D. 2009, A&A, 494, 95
Majewski, S. R. 1993, ARA&A, 31, 575
Minchev, I., & Famaey, B. 2010, ApJ, 722, 112
Munn, J., Monet, D. G., Levine, S. E., et al. 2004, AJ, 127, 3034
Munn, J., Monet, D. G., Levine, S. E., et al. 2008, AJ, 136, 895
Navarro, J. F., Abadi, M. G., Venn, K. A., Freeman, K. C., & Anguiano, B. 2011, MNRAS, 412, 1203
Nissen, P. E., & Schuster, W. J. 2010, A&A, 511, L10
Nordström, B., Mayor, M., Andersen, J., et al. 2004, A&A, 418, 989
Parker, J. E., Humphreys, R. M., & Beers, T. C. 2004, AJ, 403, 74
Quinn, P. J., Hernquist, L., & Fullagar, D. P. 1993, ApJ, 403, 74
Reddy, B. E. 2010, in IAU Symp. 265, Chemical Abundances in the Universe: Connecting First Stars to Planets, ed. K. Cunha, M. Spite, & B. Barbuy (Cambridge: Cambridge Univ. Press), 289
Reddy, B. E., Lambert, D. L., & Allende Prieto, C. 2006, MNRAS, 367, 1329
Richard, S., Brook, C. B., Martel, H., et al. 2010, MNRAS, 402, 1489
Robin, A. C., Reylé, C., Derriére, S., & Picaud, S. 2003, A&A, 409, 523
Rocha-Pinto, H. J., Rangel, R. H. O., Porto de Mello, G. F., Braganca, G. A., & Maciel, W. J. 2006, A&A, 453, L9
Roškar, R., Debattista, V. P., Quinn, T. R., Stinson, G. S., & Wadsley, J. 2008a, ApJ, 684, L79
Roškar, R., Debattista, V. P., Stinson, G. S., et al. 2008b, ApJ, 675, L65
Sales, L. V., Helmi, A., Abadi, M. G., et al. 2009, MNRAS, 400, L61
Schlesinger, K. J., Johnson, J. A., Lee, Y. S., et al. 2010, ApJ, 719, 996
Schönrich, R., & Binney, J. 2009a, MNRAS, 396, 203
Schönrich, R., & Binney, J. 2009b, MNRAS, 399, 1145
Schönrich, R., Binney, J., & Dehnen, W. 2010, MNRAS, 403, 1829
Sellwood, J. A., & Binney, J. J. 2002, MNRAS, 336, 785
Sesar, B., Ivezić, Ž., & Jurić, M. 2008, ApJ, 689, 1244
Sestito, P., Bragaglia, A., Randich, S., et al. 2008, A&A, 488, 943
Smolinski, J. P., Lee, Y. S., Beers, T. C., et al. 2011, AJ, 141, 89
Soubiran, C., Bienaymé, O., & Siebert, A. 2003, A&A, 398, 141
Soubiran, C., & Girard, P. 2005, A&A, 438, 139
Spagna, A., Lattanzi, M. G., Re Fiorentin, P., & Smart, R. L. 2010, A&A, 510, L4
Spitzer, L., & Schwarzschild, M. 1953, ApJ, 118, 106
Steinmetz, M., Zwitter, T., Siebert, A., et al. 2006, AJ, 132, 1645
Villalobos, Á., & Helmi, A. 2008, MNRAS, 391, 1806
Villalobos, Á., Kazantzidis, S., & Helmi, A. 2010, ApJ, 718, 314
Wilson, M., Helmi, A., Morrison, H. L., et al. 2011, MNRAS, 413, 2235
Wyse, R. F. G., Gilmore, G., Norris, J. E., et al. 2006, ApJ, 639, L13
Yanny, B., Rockosi, C., Newberg, H. J., et al. 2009, AJ, 137, 4377
York, D. G., Adelman, J., Anderson, J. E., Jr., et al. 2000, AJ, 120, 1579
Yoshii, Y. 1982, PASJ, 34, 365
Zwitter, T., Siebert, A., Munari, U., et al. 2008, AJ, 136, 421